LABORATORI NAZIONALI DI FRASCATI
SIS – Pubblicazioni

LNF-96/008 (IR)
14 Febbraio 1996

K_L Interactions and K_S Regeneration in KLOE

R. Baldini, A. Michetti

INFN–Laboratori Nazionali di Frascati, P.O. Box 13, I–00044 Frascati (Rome), Italy

Abstract

K_L total, elastic and K_S regeneration cross sections are evaluated at the K_L momenta from Φ decay. As far as total and elastic cross sections are concerned the results agree with the available experimental data, at slightly higher momenta. As for K_S regeneration they are rather unexpected, but unfortunately there are no experimental data available to make any check. These cross sections have been compared with the present codes for hadronic interactions in GEANT. Finally evaluations of K_S regeneration and K_L interactions on the different parts of the KLOE detector are reported.

1 Introduction

The aim of this note is to evaluate the various cross sections of K_L on nuclei at low momenta. There is a serious lack of such data at momenta below 500 MeV/c. On the other hand, in the KLOE experiment [1] at the Φ Factory DAΦNE in Frascati, since in Φ decay P_k is $\sim$ 114 MeV/c, it is important to know the K_L cross sections at such momenta; specifically:

- K_S regeneration through the detector simulates a K_L decay violating $\mathcal{CP}$, diluting the values of the $\mathcal{CP}$ parameters;
- K_L elastic and inelastic collisions through the detector affect the evaluation of various detection efficiencies;
- Finally at present the simulations can not be modeled faithfully. In particular the GEANT codes, GHEISHA and FLUKA, fail in the calculations of these K_L cross sections.

2 K_L cross sections on nucleon

The present situation concerning Kaon-nucleon amplitudes is summarized in the following. Data are available [2] on K^+ and K^- cross sections, which are related to K^0 and $\bar{K}^0$ cross sections by a rotation in the isotopic spin space:

$$\begin{aligned} A_{K_Lp\to K_Lp}(\theta) &= [A_{K^+n}(\theta) + A_{K^-n}(\theta)]/2 \\ A_{K_Ln\to K_Ln}(\theta) &= [A_{K^+p}(\theta) + A_{K^-p}(\theta)]/2 \\ A_{K_Lp\to K_Sp}(\theta) &= [A_{K^+n}(\theta) - A_{K^-n}(\theta)]/2 \\ A_{K_Ln\to K_Sn}(\theta) &= [A_{K^+p}(\theta) - A_{K^-p}(\theta)]/2 \end{aligned}$$

By the way, there is a lack of data also for charged Kaon-nucleon scattering at low momenta. All these amplitudes can be written at low momenta in terms of few partial waves ℓ and scattering lenghts $a_I(k)$, which should depend weakly on the incident momentum k:

$$T(\theta) = \sum_\ell (2\ell+1) T_\ell(k) P_\ell(cos\theta)$$

$$T_I(k) = \frac{a_I(k)}{1 - \imath k a_I(k)}$$

P GeV/c	Re[$A(K^-p)$] (fm)	Re[$A(K^-n)$] (fm)	Re[$A(K^+p)$] (fm)	Re[$A(K^+n)$] (fm)
0.00	-0.98	0.54	-0.50	-0.23
0.35	0.36	0.12	-0.48	-0.14
0.375	0.50	0.15	-0.48	-0.13
0.40	0.16	0.17	-0.48	-0.13
0.425	0.03	0.18	-0.47	-0.12
0.50	0.26	0.25	-0.46	-0.10
0.60	0.46	0.40	-0.45	-0.08
0.70	0.69	0.67	-0.43	-0.09
0.75	0.82	0.68	-0.41	-0.09
0.80	0.86	0.81	-0.35	-0.09
0.85	0.82	0.84	-0.36	-0.08
0.90	0.86	0.81	-0.35	-0.07
0.95	0.82	0.53	-0.34	-0.06
1.00	0.74	0.25	-0.34	-0.06
1.05	0.44	0.15	-0.34	-0.07
1.10	0.09	0.11	-0.35	-0.12
1.20	0.05	0.19	-0.42	-0.21
1.30	0.20	0.24	-0.48	-0.26
1.40	0.41	0.28	-0.52	-0.27
1.50	0.50	0.27	-0.56	-0.28
1.60	0.41	0.21	-0.58	-0.30
1.80	0.24	0.27	-0.62	-0.33
2.00	0.29	0.28	-0.67	-0.38
2.20	0.31	0.23	-0.72	-0.41
2.40	0.27	0.25	-0.76	-0.44
2.60	0.28	0.22	-0.81	-0.47

Table 1: Real parts of the forward $K^{\pm}$ scattering amplitude, according to A.D.Martin.

With regard, to isospin, K^-p and K^+n elastic amplitudes are superpositions of states with isotopic spin $I = 0$ and $I = 1$:

$$< K^{\pm}N|T|K^{\pm}N >= \frac{1}{2}(T_0^{\pm} + T_1^{\pm})$$

Only $I = 1$ amplitudes contribute to the transitions $K^+p \to K^+p$ and $K^-n \to K^-n$.
At $P_k \simeq 100$ MeV/c the S wave contribution is still dominant as expected, but with respect to the threshold there is a steep variation of the real part of the $I = 0$ part of the K^-N amplitude (see table 1). It is very likely that this anomaly is due to a resonance below threshold, the so called $\Lambda(1405)$, whose nature has not yet been understood [2]. Nevertheless the scattering lengths $a_I(0)$ have been calculated by means of dispersion relations. The results obtained by A.D. Martin [3] are:

$$a_I(K^-) \to \begin{cases} a_0 = (-1.70 + \imath 0.68)\ \text{fm} \\ a_1 = (0.37 + \imath 0.60)\ \text{fm} \end{cases}$$

$$\alpha_I(K^+) \to \begin{cases} \alpha_0 = 0.02\ \text{fm} \\ \alpha_1 = -0.33\ \text{fm} \end{cases}$$

K^+-nucleon scattering amplitudes must be real, due to the optical theorem, because only the elastic channel is open at threshold. On the contrary inelastic reactions, like $K^-p \to \Lambda\pi$

and $K^- p \to \Sigma\pi$, are available in the K^--nucleon case also at $k = 0$: hence Im f(0)$\neq$0 and the total K_LN cross section must behave like $1/k$ at low momenta.

According to A.D. Martin, for kaons from the Φ decay:

$$\begin{aligned} f_{K^-p} &= (-0.32 + \imath\, 0.75)\ \text{fm} \\ f_{K^-n} &= (0.24 + \imath\, 0.52)\ \text{fm} \\ f_{K^+p} &= (-0.33 + \imath\, 0.04)\ \text{fm} \\ f_{K^+n} &= (-0.15 + \imath\, 0.02)\ \text{fm} \end{aligned}$$

and the elastic and regeneration cross sections for K_L on nucleon, assuming isotropic angular distributions, are :

$$\begin{aligned} \sigma_{el}^{K_L p} &= |f_{el}^{K_L p}|^2 \cdot 4\pi \simeq 9\ \text{mb} \\ \sigma_{el}^{K_L n} &= |f_{el}^{K_L n}|^2 \cdot 4\pi \simeq 32\ \text{mb} \\ \sigma_{reg}^{K_L p} &= |f_{reg}^{K_L p}|^2 \cdot 4\pi \simeq 13\ \text{mb} \\ \sigma_{reg}^{K_L n} &= |f_{reg}^{K_L n}|^2 \cdot 4\pi \simeq 16\ \text{mb} \end{aligned}$$

The cross sections on deuteron (neglecting shadow and Fermi motion effects) are

$$\begin{aligned} \sigma_{el}^{K_L D} &\approx 42\ \text{mb} \\ \sigma_{reg}^{K_L D} &\approx 28\ \text{mb} \end{aligned}$$

"Errors" can be given to these cross sections computing them according to other authors [4, 5, 6], as shown in table 2. These "errors" range from 10% to 30 %: hence it is not worthwhile to pursue an accuracy to better than $\approx$ 20 % in estimating of the K_L cross sections on nuclei. It is very likely that these large uncertainties are related to the anomalous variation near threshold of the real part of the $I = 0$ K_LN amplitude as mentioned before. The total $K_L p$ cross section, according to the A.D. Martin's parametrization, as a function of the K_L momentum is shown in fig.1 in comparison with some experimental data.

Charged kaons and neutral kaons have been related each other by a rotation in the isotopic space assuming the difference in kaon masses is negligible. However the mass difference (4 MeV/c^2) is of the same order of magnitude of the kinetic energies of the kaons in the Φ decay and it could alter the situation. R.H. Dalitz evaluated the scattering amplitude K^-N taking into account the mass difference properly [7]:

$$f_{K^-N} = \left(\frac{\frac{1}{2}(a_0 + a_1) - \imath k_0 a_1 a_0}{1 - \frac{1}{2}(a_1 + a_0)(k + k_0) - k k_0 a_0 a_1} \right)$$

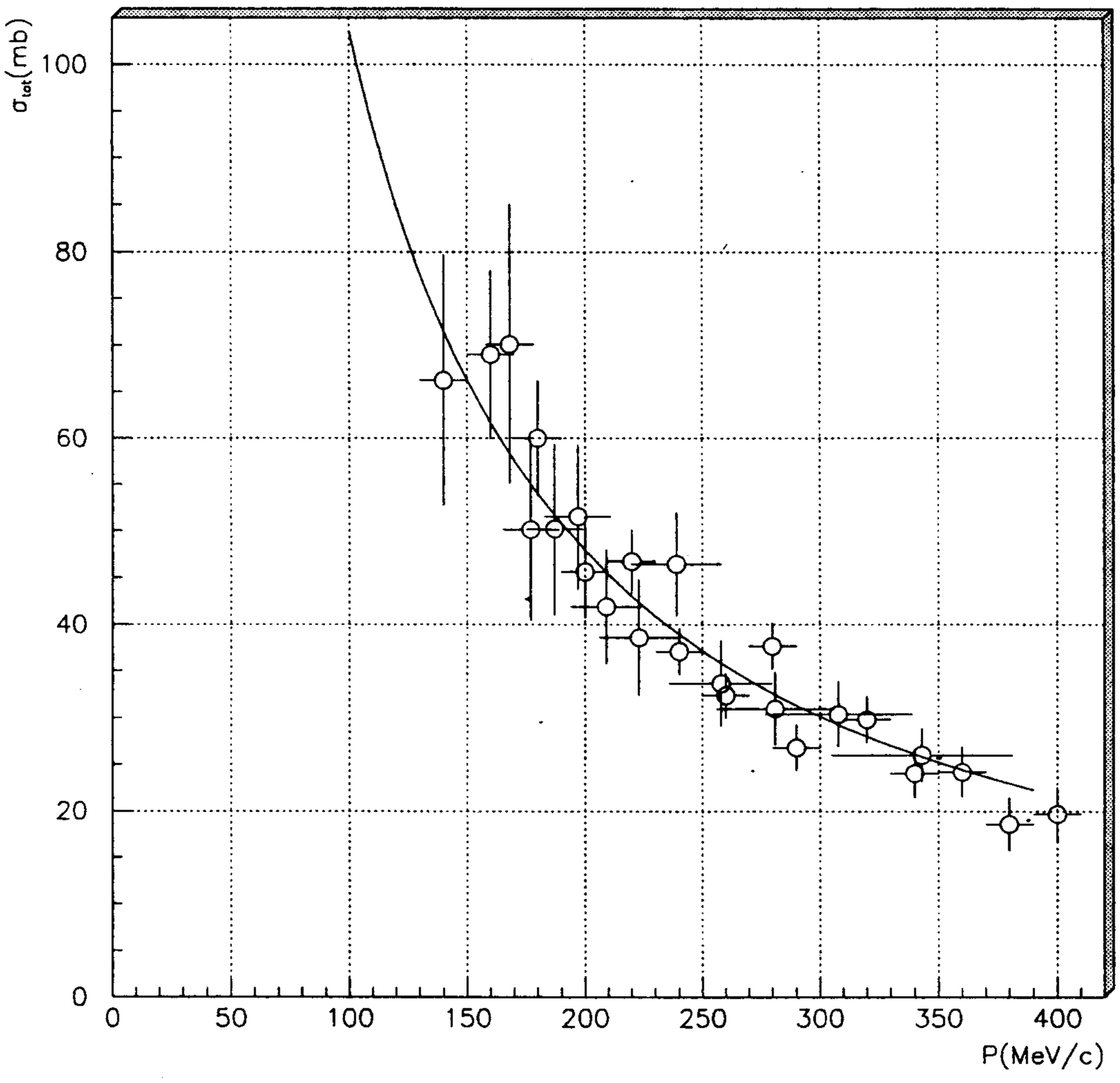

Figure 1: Comparison of total cross section $K_L p$ to Martin calculation.

Author	$\sigma_{el}^{K_L p}$ (mb)	$\sigma_{el}^{K_L n}$ (mb)	$\sigma_{reg}^{K_L p}$ (mb)	$\sigma_{reg}^{K_L n}$ (mb)
Kim [4]	11.2	38.4	8.9	16.7
Dalitz [5]	7.5	30.4	9.6	14.3
Martin [3]	9.3	32.0	12.7	15.7
Conboy [6]	18.6	40.4	11.0	16.2
Mean	11.7 ± 4.2	35.3 ± 4.2	10.6 ± 1.4	15.7 ± 0.9
Martin $\pm$ *Error*	9.3 ± 3.3	32.0 ± 3.8	12.7 ± 1.7	15.7 ± 0.9

Table 2: $\sigma(K_L \mathrm{N})$: Comparison between the cross sections, at $P_k = 114$ MeV/c, as obtained by different authors.

where

$$k_0^2 = k^2 - 2\frac{m_K M_N}{m_K + M_N}(m_{K^0} - m_{K^-}).$$

In table 3 this correction on the total $K^- p$ cross section is reported. It appears to be negligible at our momenta.

3 K_L total cross sections on heavy nuclei

Experimental data exist on K_L total cross sections on different nuclei at low momenta, ranging from 168 MeV/c up to 343 MeV/c [8], and they are shown in table 4. These data have been fitted as a function of atomic number A by means of a power law $\sigma_{tot} = C \cdot \mathrm{A}^{\alpha}$, also while looking for simple extrapolations and interpolations to other nuclei. The results are shown in fig.2 and shown in table 5.

From these pictures an anomaly appears in the cross section on Cu. However, apart from this nucleus, these data show a reasonable agreement with this simple fit.

The parameter α has to be compared with the black disk prediction $\alpha \simeq 0.67$. Scattering on a black disk is a qualitative description of any hadronic interaction on heavy nuclei. A nucleus may be considered a black disk, with radius $R = r_0 \, \mathrm{A}^{1/3}$ and $r_0 \simeq 1.1$ fm, if the total cross section on nucleon is at least $\approx \pi r_0^2 \simeq 30$ mb. It may be worthwile to recall the

P MeV/c	$\sigma(K^-p)$ (mb)	$\Delta\sigma$ (mb)
30	912.5	13.9
50	569.0	3.7
70	412.8	1.4
90	320.9	0.6
110	259.6	0.3
130	215.7	0.2
150	182.6	0.1
170	157.0	0.1
190	136.6	0.0
210	120.2	0.0
230	106.7	0.0

Table 3: Total cross section for K^-p interaction with corrections due to mass difference.

P Mev/c	H (mb)	Be (mb)	C (mb)	Al (mb)	Fe (b)	Cu (b)	Pb (b)
168	70.1 ± 15.0	476 ± 37	481 ± 24	963 ± 89	1.54 ± 0.47	1.31 ± 0.19	3.55 ± 0.41
177	50.1 ± 9.7	355 ± 23	445 ± 21	722 ± 52	1.08 ± 0.10	1.17 ± 0.11	3.62 ± 0.30
187	50.2 ± 9.2	385 ± 22	477 ± 18	860 ± 55	1.50 ± 0.24	1.37 ± 0.12	3.35 ± 0.24
197	51.5 ± 7.8	390 ± 20	456 ± 15	845 ± 51	1.46 ± 0.23	1.39 ± 0.13	3.73 ± 0.27
209	41.9 ± 6.1	341 ± 16	430 ± 14	799 ± 41	1.19 ± 0.10	1.19 ± 0.08	3.32 ± 0.19
223	38.6 ± 6.2	332 ± 16	429 ± 14	850 ± 46	1.51 ± 0.30	1.21 ± 0.11	3.54 ± 0.24
239	46.4 ± 5.5	311 ± 14	411 ± 12	793 ± 38	1.29 ± 0.15	1.25 ± 0.09	3.67 ± 0.22
258	33.7 ± 4.6	316 ± 14	391 ± 11	750 ± 35	1.14 ± 0.07	1.23 ± 0.10	3.09 ± 0.16
281	31.0 ± 3.9	265 ± 12	361 ± 9	703 ± 31	1.41 ± 0.15	1.111 ± 0.062	3.40 ± 0.18
308	30.4 ± 3.5	269 ± 11	336 ± 8	683 ± 29	1.24 ± 0.11	1.146 ± 0.060	3.26 ± 0.17
343	26.0 ± 2.9	242 ± 10	308 ± 7	638 ± 26	1.18 ± 0.08	0.969 ± 0.044	3.14 ± 0.14

Table 4: Experimental total cross sections of K_L on different nuclei.

P MeV/c	C (mb)	α	$\sigma_{tot}(K_L He)$ (mb)
168	91 ±2	0.69 ±0.01	236 ± 6
177	71 ±3	0.72 ±0.01	190 ± 10
187	81 ±3	0.71 ±0.01	220 ± 10
343	41 ±9	0.81 ±0.01	130 ± 30

Table 5: Parameters of the interpolation CA^{α} and extrapolated He cross section.

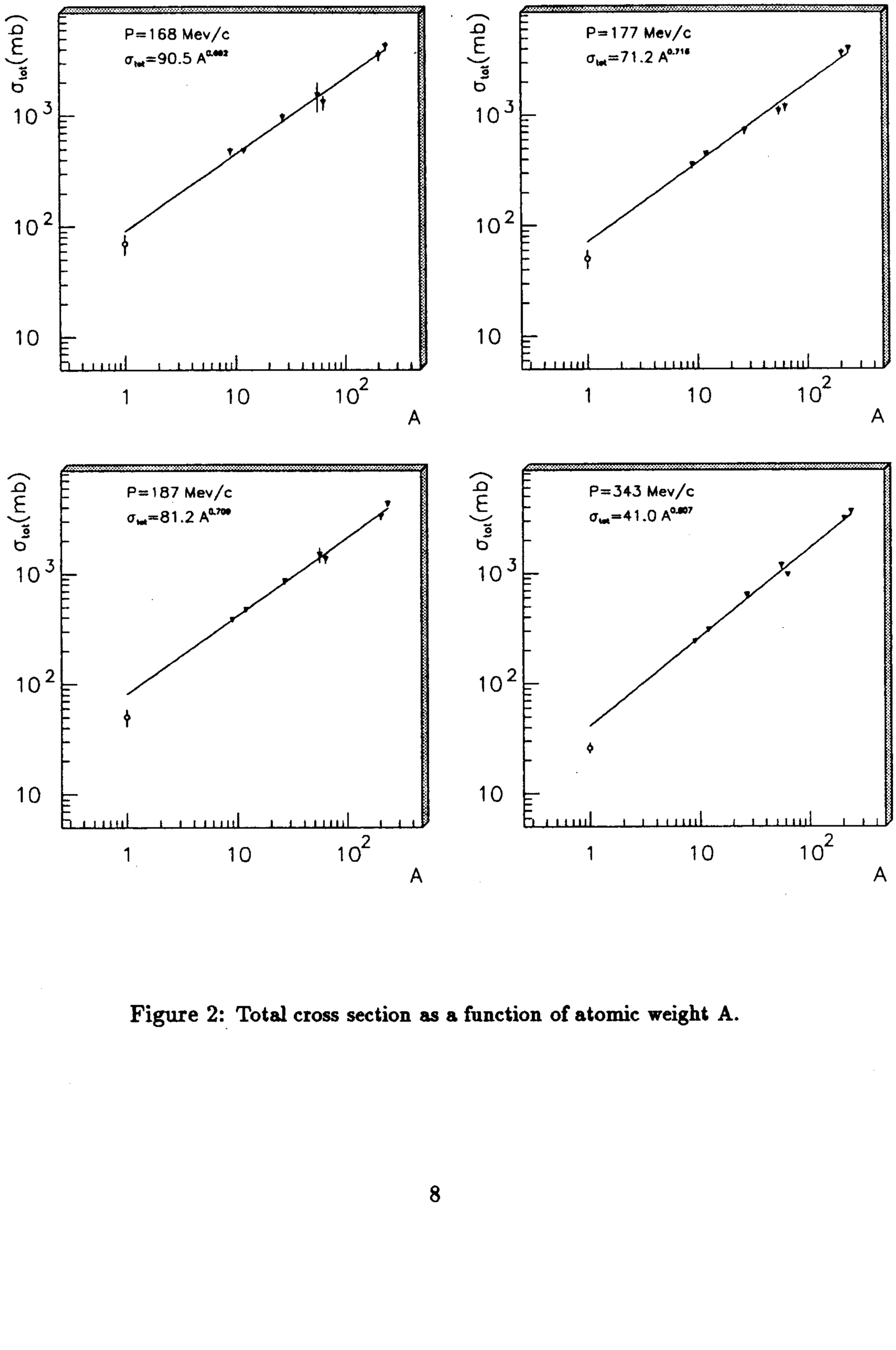

Figure 2: Total cross section as a function of atomic weight A.

	A	R_0 (fm)	σ (fm)	C (fm^{-3})	References	
He	4	1.74	0.5	0.100	$1.1A^{1/3}$	–
Be	9	2.08	0.5	0.152	$1.1A^{1/3}$	–
C	12	2.29	0.5	0.162	$1.1A^{1/3}$	–
Al	27	2.84	0.569	0.201	Fey 1973	[13]
Fe	56	3.98	0.569	0.177	Fey 1973	[13]
Cu	64	4.214	0.586	0.170	Gompelman 1976	[14]
Pb	207	6.62	0.546	0.160	de Jager 1973	[14]

Table 6: Parameters used in Wood-Saxon distribution.

main results of the black disk model, as a basis for any more refined model:

- $\sigma_{tot} \simeq 2\,\sigma_{el} \simeq 2\pi r_0^2 \mathrm{A}^{2/3}$.
- $\sigma_{tot} \simeq$ independent of the incoming momentum k.
- $\Delta\cos\theta \simeq 2/(k^2R^2)$

K^-N cross sections are in the black disk regime, but K^+N cross sections at low momenta are rather smaller.

A more refined, but still very elementary model, that is the eikonal approximation (E.A.), is considered from now on. According to the E.A. the scattering amplitude on a nucleus at high energies and at small angles is given by

$$f(\theta) = \frac{k}{i}\int_0^\infty \left[e^{i\chi(b)-1}\right] J_0(kbsin\theta)\; b\; db$$

where

$$\chi(\vec{b}) = \frac{1}{\mathrm{A}}\left[\mathrm{Z}a^p(0) + (\mathrm{A\text{-}Z})a^n(0)\right]\frac{4\pi}{k}\int_0^{+\infty} R(\sqrt{b^2+z^2})\; dz$$

$a^p(0)$ and $a^n(0)$ are the forward K_L elastic scattering amplitudes on proton and neutron respectively, while the function R(r) represents the matter distribution inside the nucleus. According to the Wood-Saxon distribution, with the parameters in table 6, it is:

$$R(r) = \frac{C}{1+\exp[(r-R_0)/\sigma]}$$

Therefore by means of the E.A. and the forward scattering amplitude on nucleon the scattering amplitude on nucleus is obtained.

From now on the E.A. will be assumed to be a good approximation also at low kaon momenta (P$\approx$ 100 MeV/c). As mentioned before this approximation is valid at high energies, if several partial waves are involved (that is if $kR \gg 1$), furthermore if the forward scattering amplitude is mainly imaginary.

As a matter of fact, people make use of it successfully at much lower energies. For instance Weise [9] has compared the E.A. prediction and the available experimental data of K^+C scattering at $\simeq$ 500 MeV/c, wondering for $\simeq$ 10 % discrepancy (these controversial data are inconsistent at this level with the expectation of screening effects in a nucleus).

The E.A. is consistent with the optical theorem. Therefore not only the forward elastic amplitude, but also the total cross section, is described in this approximation.

In fig. 3 the total cross sections according to the eikonal approximation are shown in comparison with experimental data. The agreement is very good, only a significative discrepancy, still for copper, persists.

4 K_L interactions in Helium

Data on He, concerning K^-He elastic scattering at $P = 125 \div 175$ MeV/c [11], are available.

Taking into account Coulomb and strong amplitudes it is

$$f(\theta) = f_c(\theta) + f_N(\theta)$$

where:

$$f_c(\theta) = \frac{1}{k}\sum(2l+1)\left(\frac{\exp(2\imath\sigma_l)-1}{2\imath}\right)P_l(cos\theta)$$

$$f_N(\theta) = \frac{1}{k}\sum(2l+1)\exp(2\imath\sigma_l)\left(\frac{\exp(2\imath\delta_l)-1}{2\imath}\right)P_l(cos\theta)$$

The Coulomb contribution has been computed, the strong phase shifts δ_l has been extracted from these data, as shown in table 7.

There is a qualitative agreement, within large errors, between experiment and E.A. also concerning the K^-He angular distribution (see fig. 5). If anything the experimental angular distribution is shrunk with respect to the theoretical expectations, strengthening the E.A. method.

To obtain the K_L total cross section on He to be compared to the extrapolation done before by means of the experimental data of total K_L cross sections, the K^+He amplitude

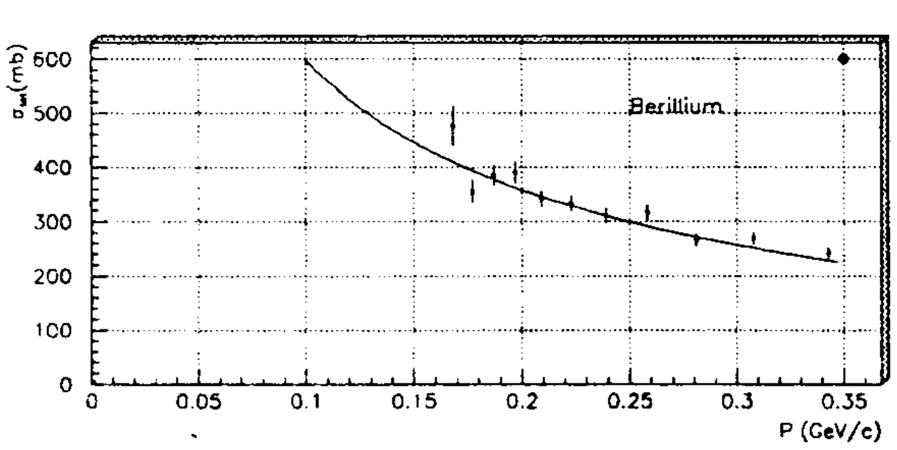

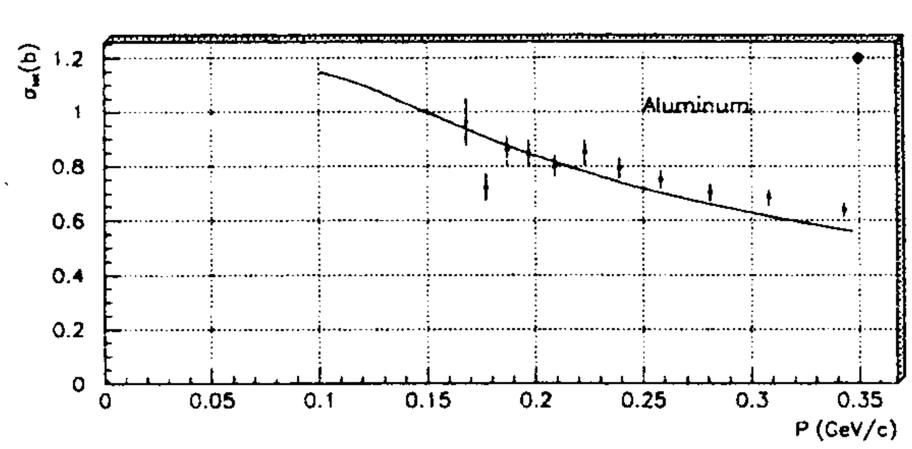

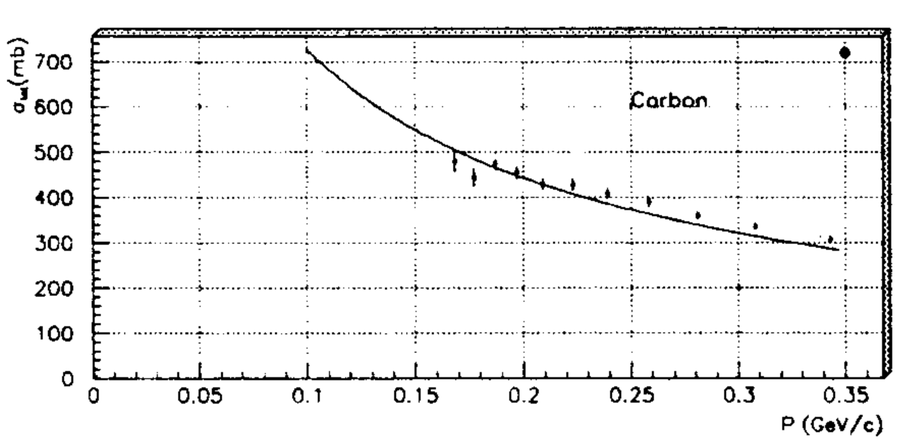

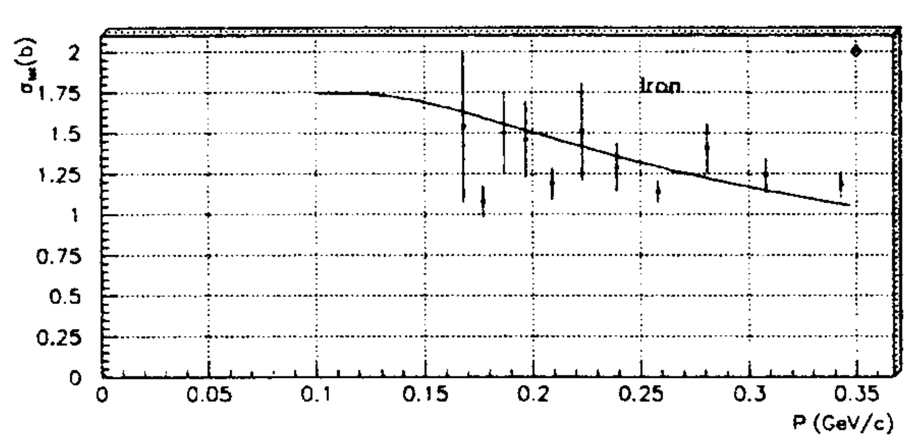

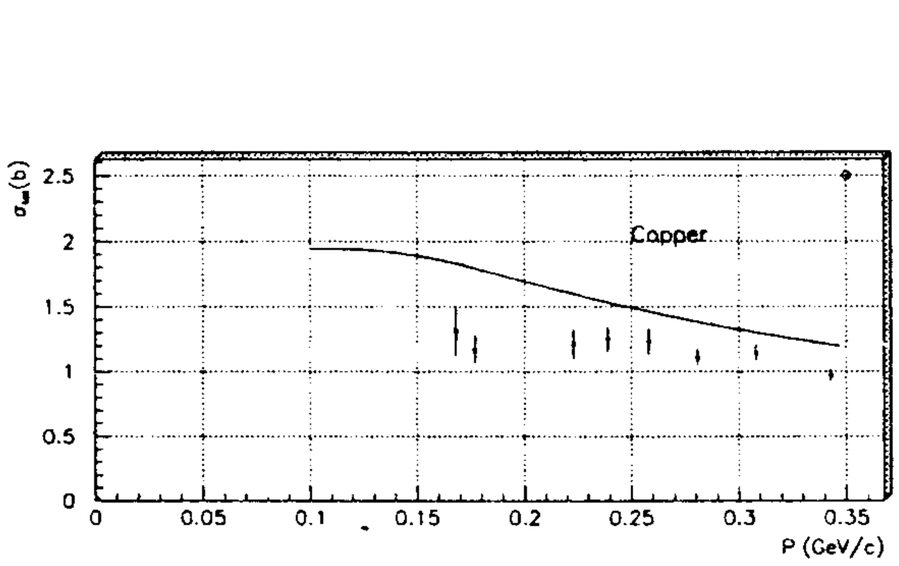

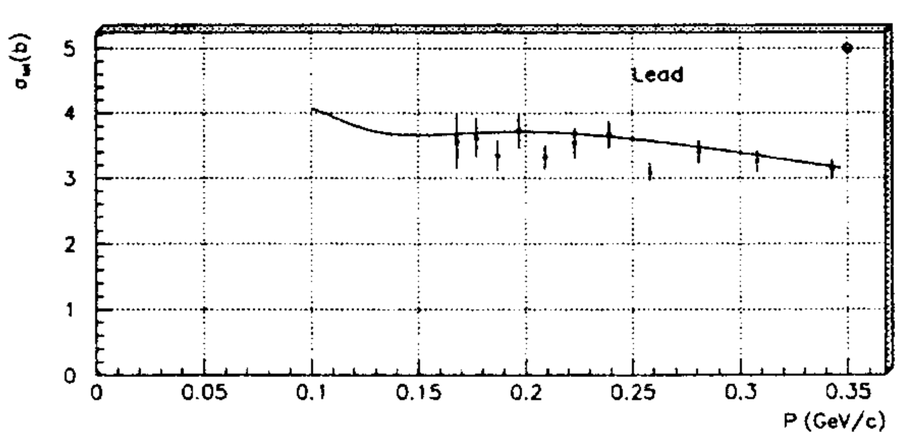

Figure 3: Comparison between experimental and theoretical total cross sections for different elements.

	P=100 ÷ 150 MeV/c		P=150 ÷ 200 MeV/c	
$\mathrm{Re}\delta_0$	-39.2	± 11.3	-36.3	± 6.7
$\mathrm{Im}\delta_0$	7.0	$^{+27.4}_{-7.0}$	4.4	$^{+9.2}_{-4.4}$
$\mathrm{Re}\delta_1$	-9.8	± 14.7	-20.4	± 6.5
$\mathrm{Im}\delta_1$	15.8	± 14.0	16.9	± 11.2
$\mathrm{Re}\delta_2$		–	-1.7	± 3.4
$\mathrm{Im}\delta_2$		–	9.1	± 4.4

Table 7: Phase shift K^-He interaction.

Momentum	$\sigma_{tot}(K_L,\mathrm{He})$ (mb)	$\sigma_{el}(K_L,\mathrm{He})$ (mb)	$\sigma_{anel}(K_L,\mathrm{He})$ (mb)	$\sigma_{reg}(K_L,\mathrm{He})$ (mb)
$P = 125 \pm 25$ MeV/c	280 ± 130	110 ± 46	170 ± 84	30 ± 18
$P = 175 \pm 25$ MeV/c	200 ± 68	75 ± 19	125 ± 48	14 ± 8
$P = 150$ MeV/c (*exp.*)	217 ± 60	80 ± 18	141 ± 31	16.6 ± 7.3
$P = 150$ MeV/c (*theor.*)	220 ± 44	66 ± 13	158 ± 32	25.9 ± 5.2

Table 8: Cross section K_LHe.

is needed also. The E.A. may provide the K^+He amplitude with enough accuracy, taking into account it is expected to be quite smaller than the K^-He amplitude. In fig. 4, K^+He and K^-He angular distributions are shown with their relative weights.

Assuming a linear dependence of the cross sections in these momenta range, an improved experimental value at P=150 MeV/c is obtained as a mean weight of the experimental cross sections at near by momenta. The comparison is shown in table 8.

5 The elastic cross section

The fact that several experimental total cross sections agree with the eikonal approximation evaluations demonstrates that the imaginary part of the forward elastic amplitude is correct.

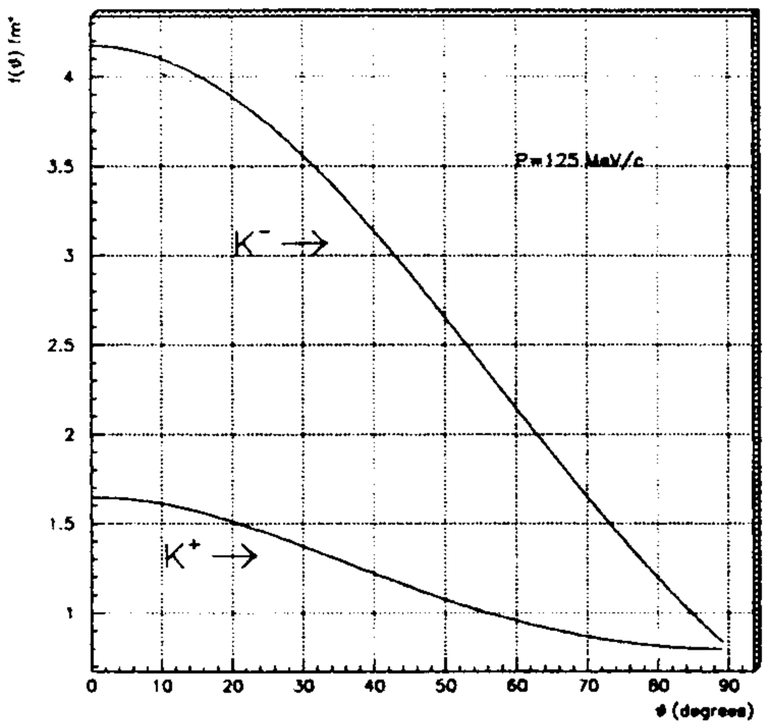

Figure 4: Comparison of angular distribuition K^+He, K^-He at P=125 MeV/c according to E.A..

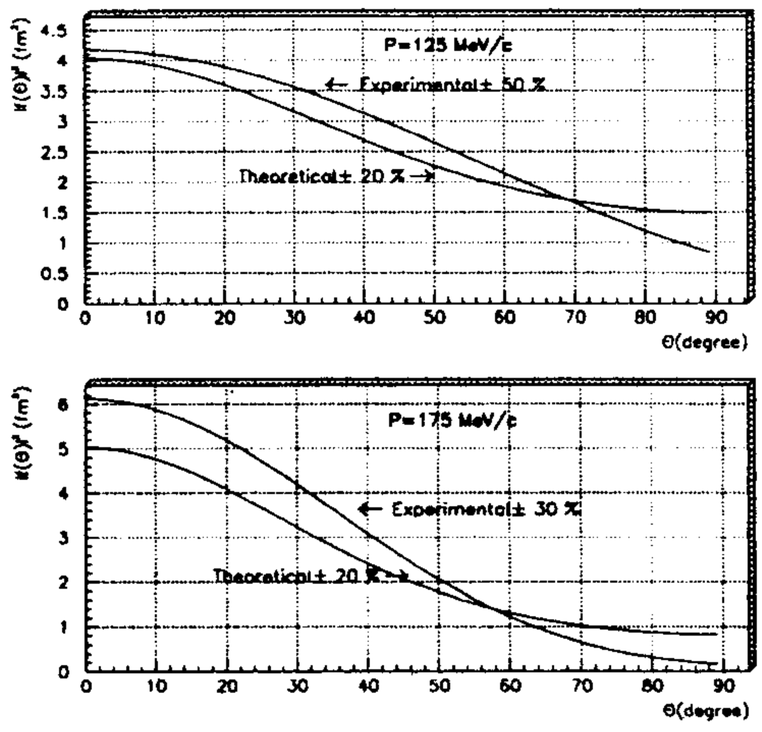

Figure 5: Comparison of theoretical and experimental K^- He elastic cross section at P=125÷175 MeV/c.

Assuming that the E.A. is valid at angles different from zero and for the real part also, the elastic cross section is given by:

$$\frac{d\sigma_{el}}{d\Omega} = \left| \frac{f(\theta) + \bar{f}(\theta)}{2} \right|^2$$

where it is assumed $f(\theta) = 0$ for $\theta > \pi/2$.

In figure 6 and 7 the angular distributions for some nuclei, at P=500 MeV/c and P=114 MeV/c, are shown. It appears that the assumption of small angles is well justified at P $\simeq$ 500 MeV/c, but becomes critical at lower momenta and for light nuclei. Therefore the eikonal approximation can not be accepted without any verification in the evaluation of the elastic scattering at angles different from zero.

6 Another approach to the K_L elastic cross section

Another approach to obtain the elastic cross section, independent of the E.A., is described in the following. In fact the imaginary part of the forward elastic amplitude can be obtained using the optical theorem, from the experimental total cross sections. It can be interpolated by a straight line, as shown in tab. 9 and shown in fig. 8. Also on nuclei it is expected at

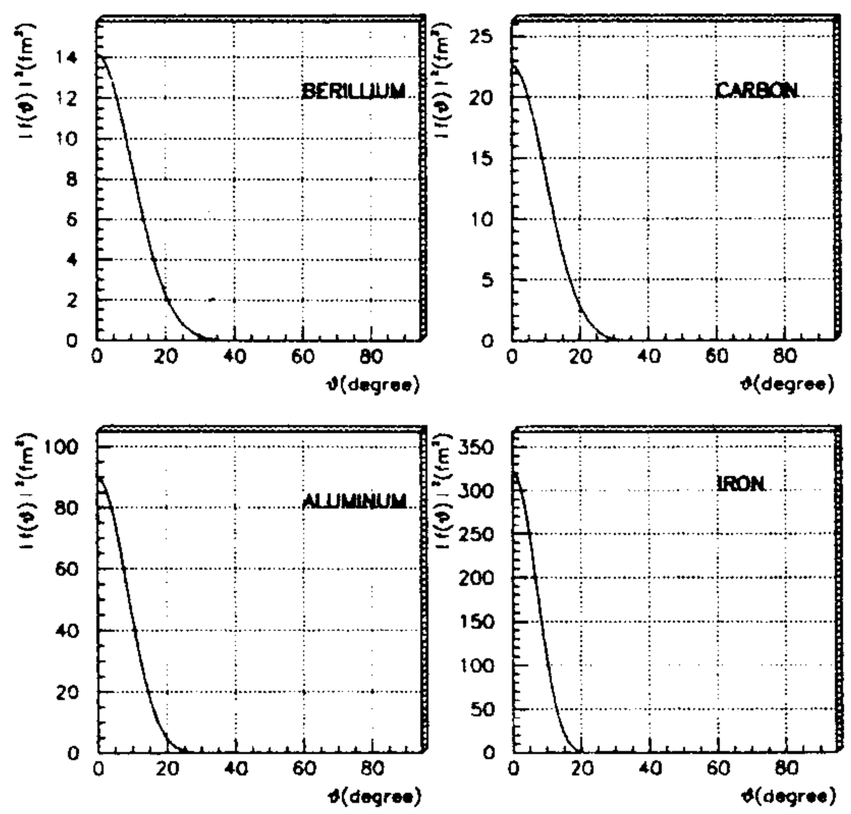

Figure 6: Angular distribution from E.A. for elastic scattering at P=500 MeV/c.

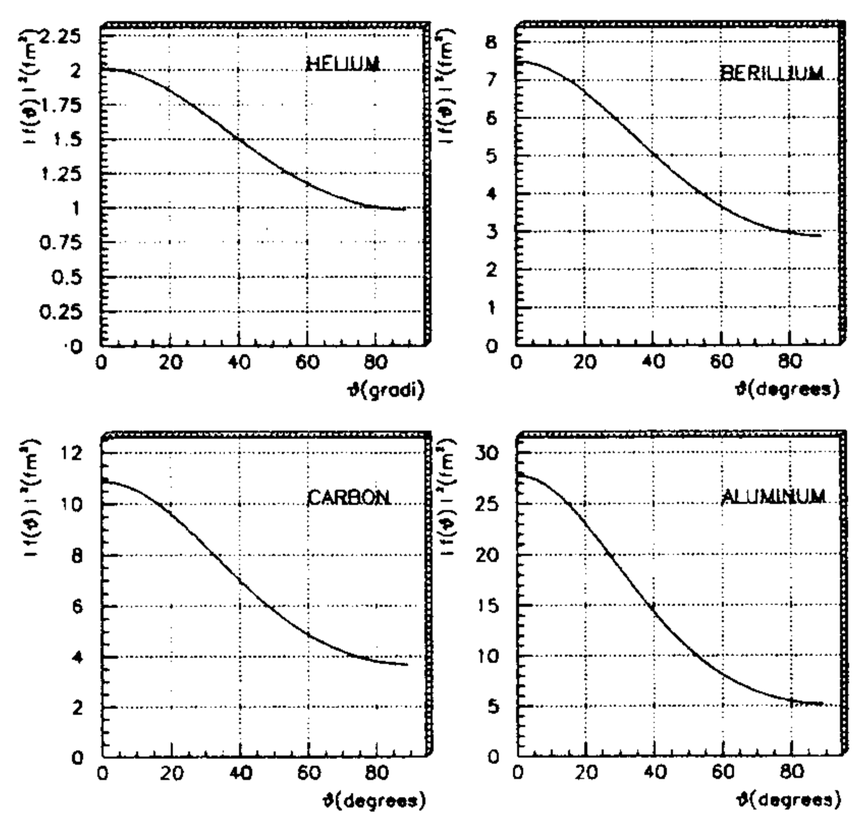

Figure 7: Angular distribution from E.A. for K_L elastic scattering at P=114 MeV/c.

Nucleus	a (fm^2)	b (GeV $\cdot fm^2$)	$\sigma_{tot}^{exp}(K_L A)$ (barn)	$\sigma_{eik}^{teo}(K_L A)$ (barn)
Be	7.8 ±2.1	5.67 ± 0.52	0.575 ± 0.067	0.544 ± 0.054
C	13.3 ±1.6	6.29 ± 0.40	0.685 ± 0.050	0.666 ± 0.067
Al	43.7 ±5.4	7.6 ± 1.3	1.11 ± 0.17	1.115 ± 0.011
Fe	123 ±16	-0.70 ± 3.9	1.17 ± 0.51	1.744 ± 0.017
Cu	71 ±11	11.2 ± 2.7	1.68 ± 0.35	1.940 ± 0.019
Pb	277±29	14.2 ± 5.1	4.01 ± 0.74	3.884 ± 0.039

Table 9: Interpolation parameters K_L-Nucleus of Im f(0).

low momenta that:

$$\mathrm{Im}f(0) = \alpha k + \beta.$$

From this linear extrapolation, the total elastic cross section at $k = 0$ is achieved, assuming that at $k = 0$ the angular distribution is strictly isotropic and the real part is small:

$$\sigma_{el} = 4\pi|\mathrm{f}(0)|^2 \simeq 4\pi|\beta|^2$$

. In fig. 9 the ratio of real to imaginary parts as obtained from E.A. is shown and it is small as expected. However also, if the real part is as large as 30% of imaginary part, the relative error on the elastic cross section would be 9% only, which is negligible with respect to the expected overall accuracy.

The first and second derivatives of the elastic K_L cross section on nuclei at small k may also be obtained. In fact, an effective range development can be carried out for the elastic amplitude for different angular momenta. At the lowest order, considering S and P waves only:

$$f_{el} = \frac{1}{\alpha_0 + \imath\beta_0 - \imath k} + \frac{3}{(\alpha_1 + \imath\beta_1)/k^2 - \imath k}.$$

The order of magnitude of α_1 and β_1 can be obtained by making a fit of the experimental data to the imaginary part of the forward elastic amplitude. The results are shown in tab. 10.

In conclusion the total K_L elastic cross section at threshold and its first and second derivatives are obtained by this approach. On the other hand the E.A. should be reliable at momenta higher than P $\simeq$ 500 MeV/c. The intermediate region can be filled connecting by

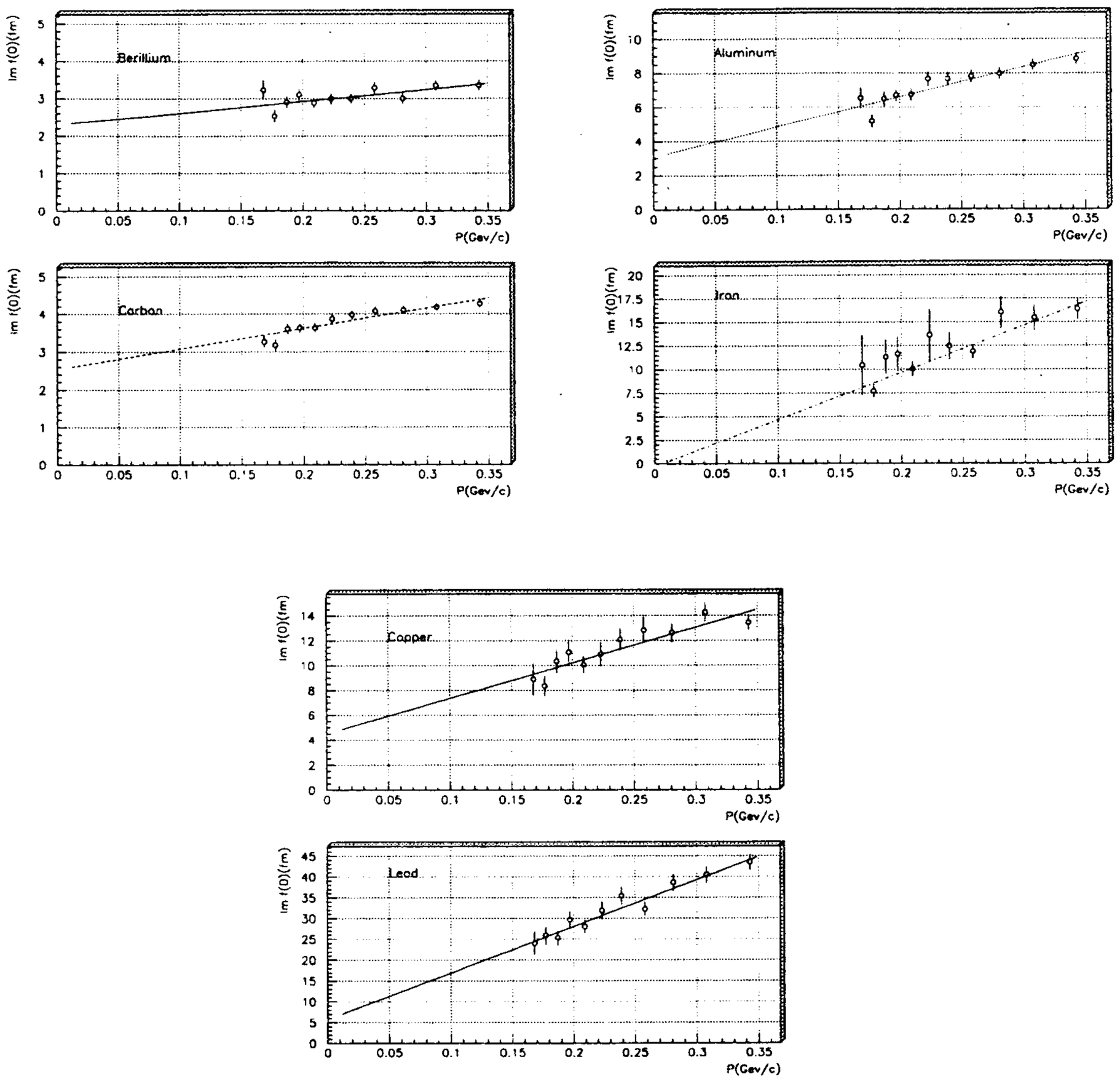

Figure 8: Im f(0) for K_L interaction on different nuclei.

Nucleus	α_0 10^{-2}fm^{-1}	β_0 fm^{-1}	α_1 fm^{-3}	β_1 fm^{-3}	Range (MeV/c)
Be	8.4	-0.4	0	-0.20	$0 \div 60$
C	7.6	-0.4	0	-0.1	$0 \div 45$
Al	6.3	-0.3	0	-0.04	$0 \div 30$

Table 10: Parameters used for the calculation of elastic cross section at low momenta.

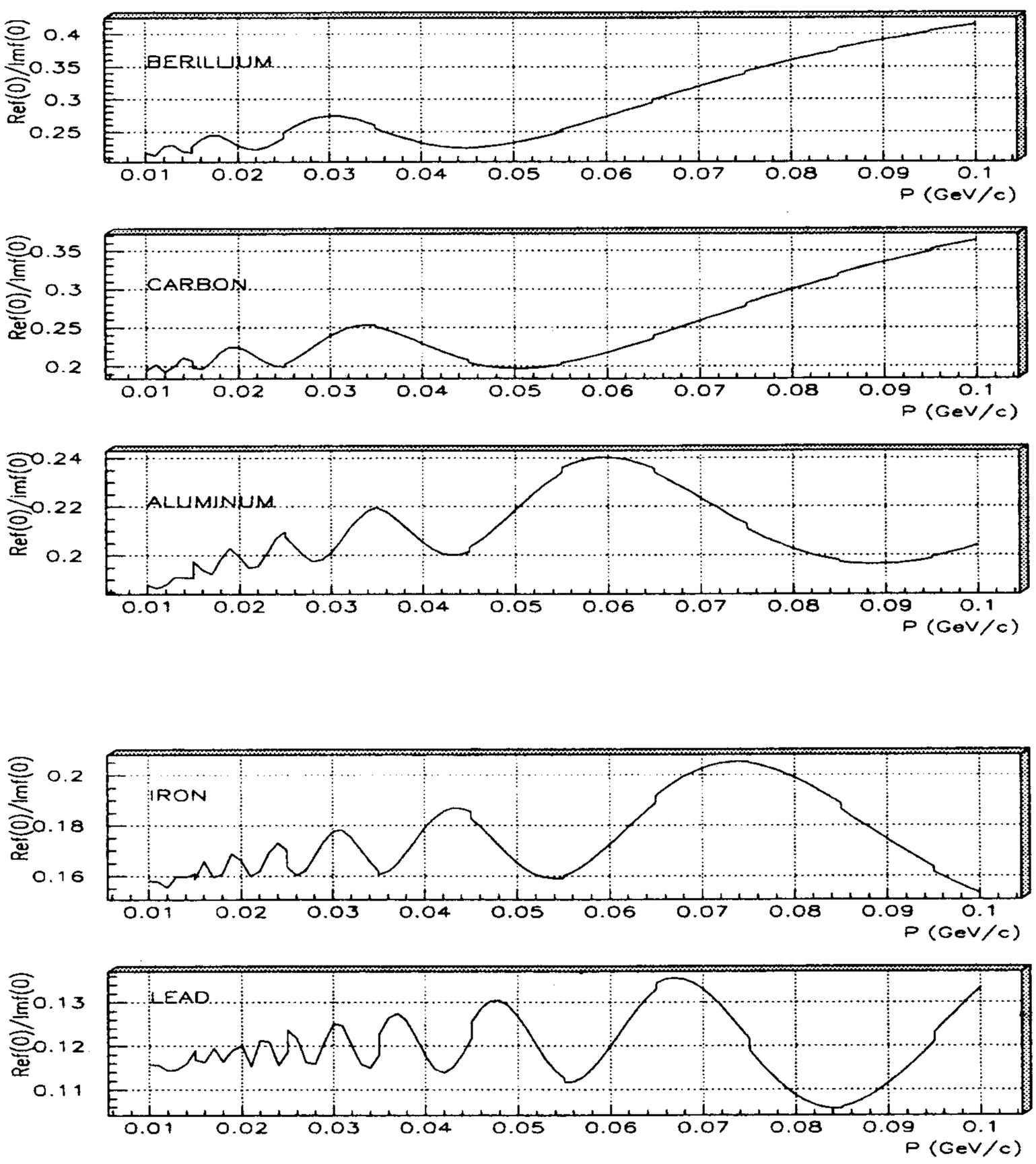

Figure 9: Ratio Re f(0)/Imf(0) from E.A. at P=10÷100 MeV/c.

a cubic spline of these two momenta regions. The results are shown (dashed line) in figg. 10,11 and 12. A 20% error has been assigned everywhere. At low momenta the S wave and the S + P waves contributions are also shown.
Some important conclusions can be drawn from these pictures:

- Elastic cross sections achieved by these cubic splines are consistent with the E.A., within errors.

- The S wave contribution is below the E.A. values as expected.

These results and the elastic K^- cross section on He support the E.A. for the evaluation of the K_L elastic scattering on nuclei at $P_k \sim 150$ MeV/c.

7 The K_L regeneration cross section

The regeneration amplitude is related to the $\bar{K}^0$ and K^0 (or K^- and K^+) elastic amplitudes by the relation:

$$f_{reg}(\theta) = \frac{f^+(\theta) - f^-(\theta)}{2} \tag{1}$$

At present the only data available at low momenta are the forward regeneration amplitude on Cu, down to 600 MeV/c [10] and they agree with E.A., within the 10% estimated accuracy in the amplitude calculation (see fig. 14). As mentioned before, on Helium there is agreement between experimental data end eikonal approximation within trhe quoted errors. On Be, CMD2 has recently measured

$$\sigma_{reg}^{Be} = 63 \pm 19\text{mb} \tag{2}$$

This value has to be compared with the E.A. prediction

$$\sigma_{reg}^{Be} = 41 \pm 8\text{mb} \tag{3}$$

In fig. 13 their angular distribution is reported and compared with the E.A. expectation. Actually CMD2 has measured the angular distribution projected on the plane orthogonal to the beam axis. The angular distribution is extracted in the hypotesis of a flat acceptance

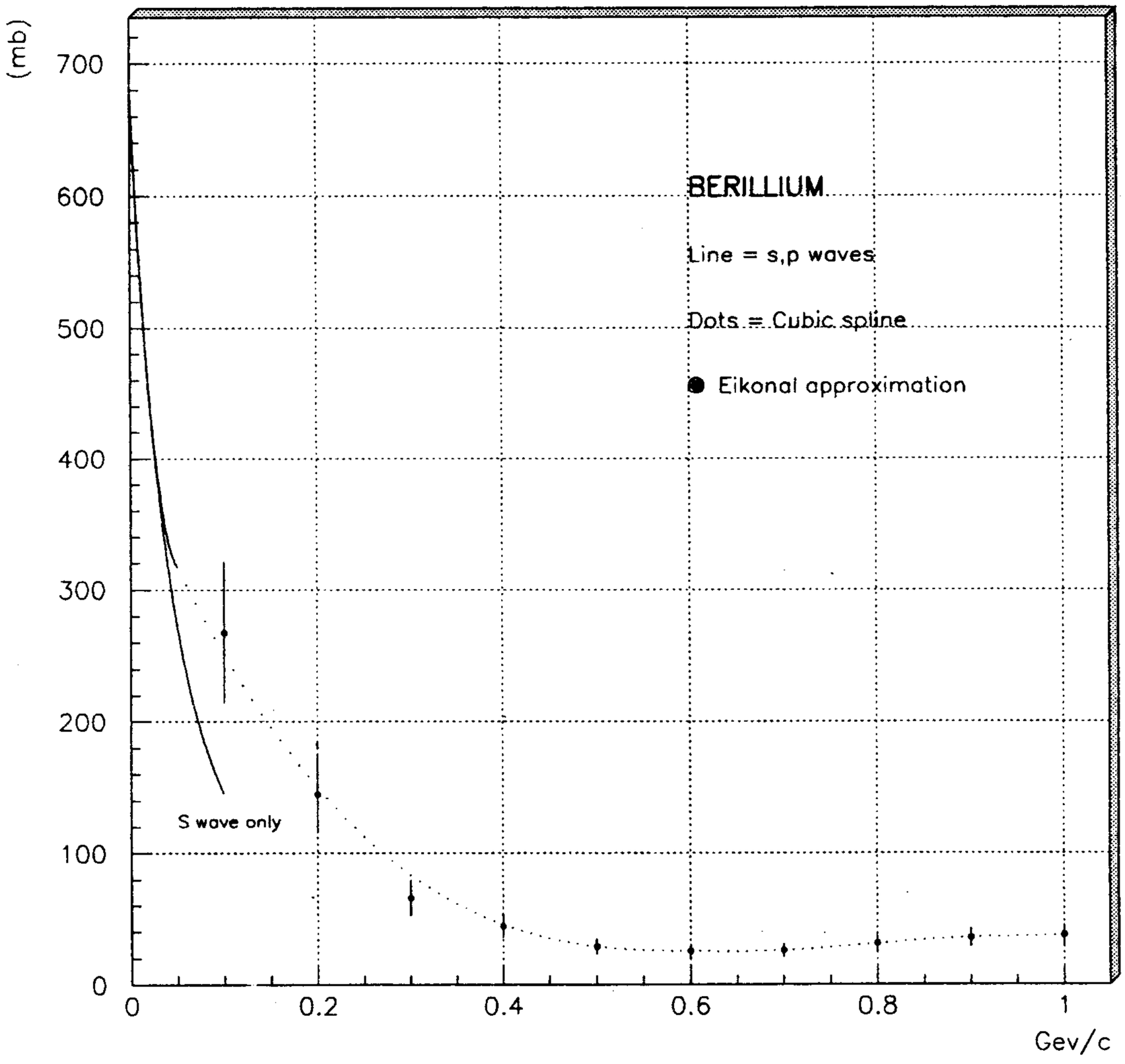

Figure 10: Elastic cross section K_L Be in the range P=0 ÷1 GeV/c.

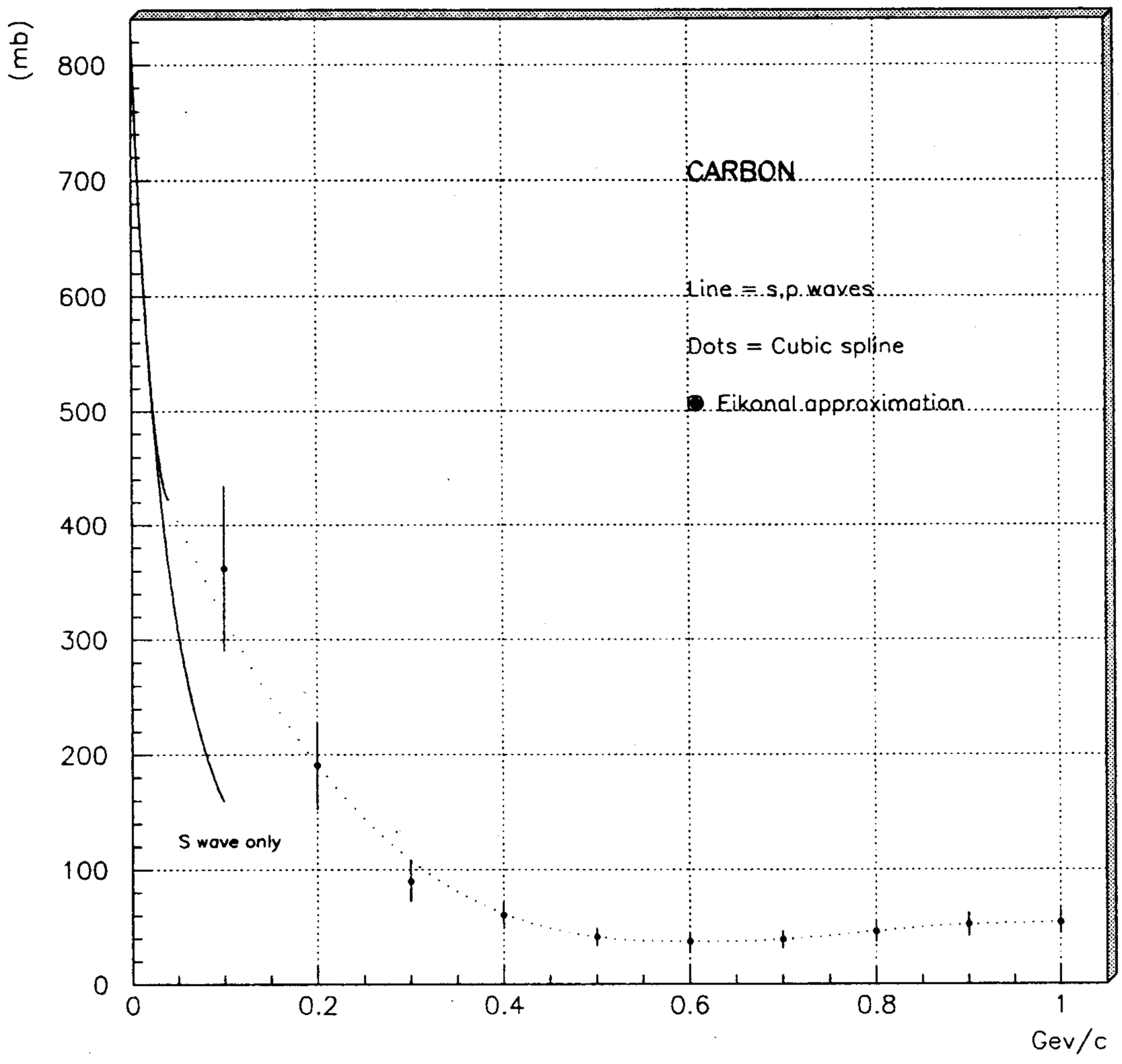

Figure 11: Elastic cross section K_L C in the range P=0 ÷1 GeV/c.

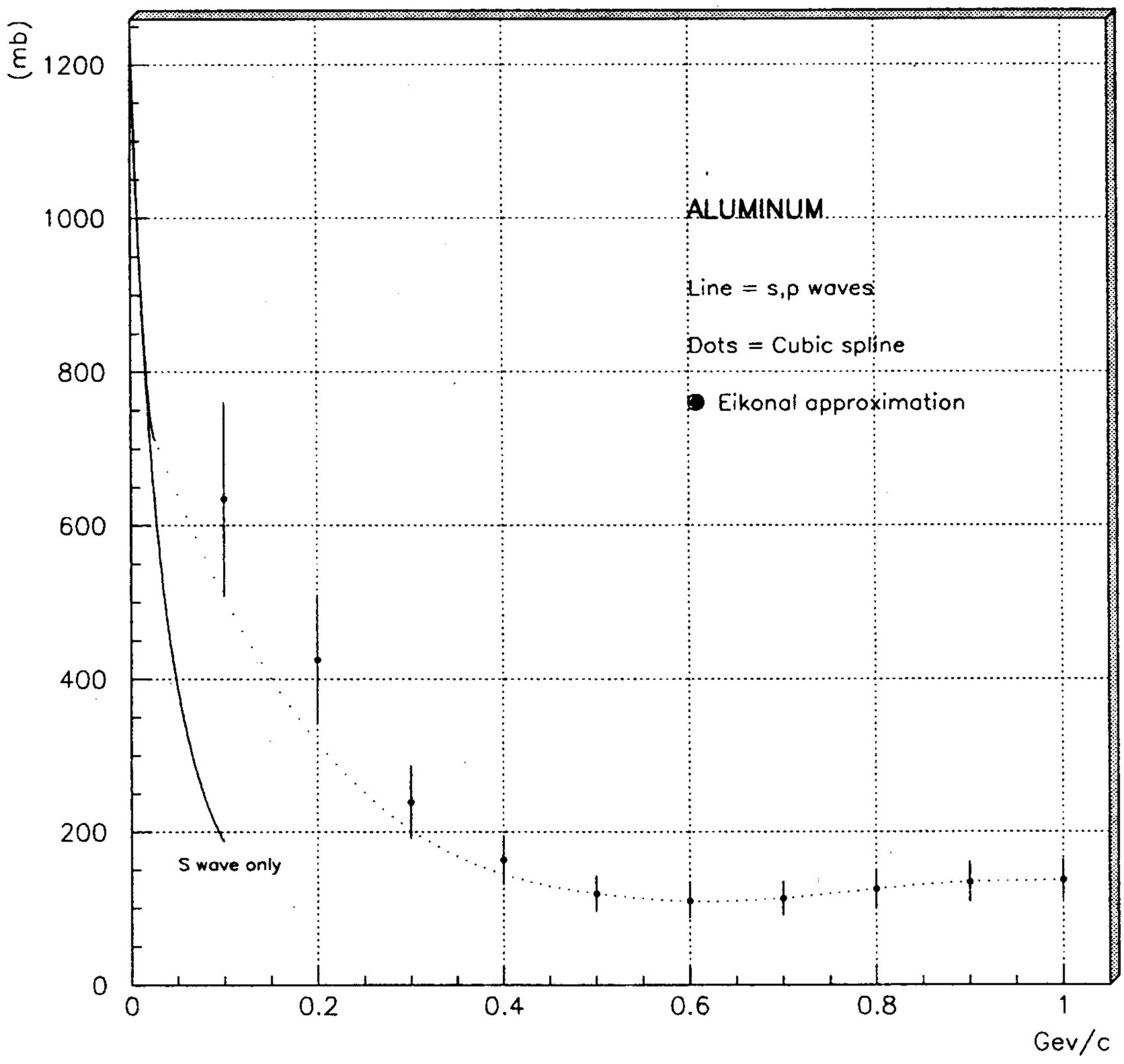

Figure 12: Elastic cross section K_L Al in the range P=0 ÷1 GeV/c.

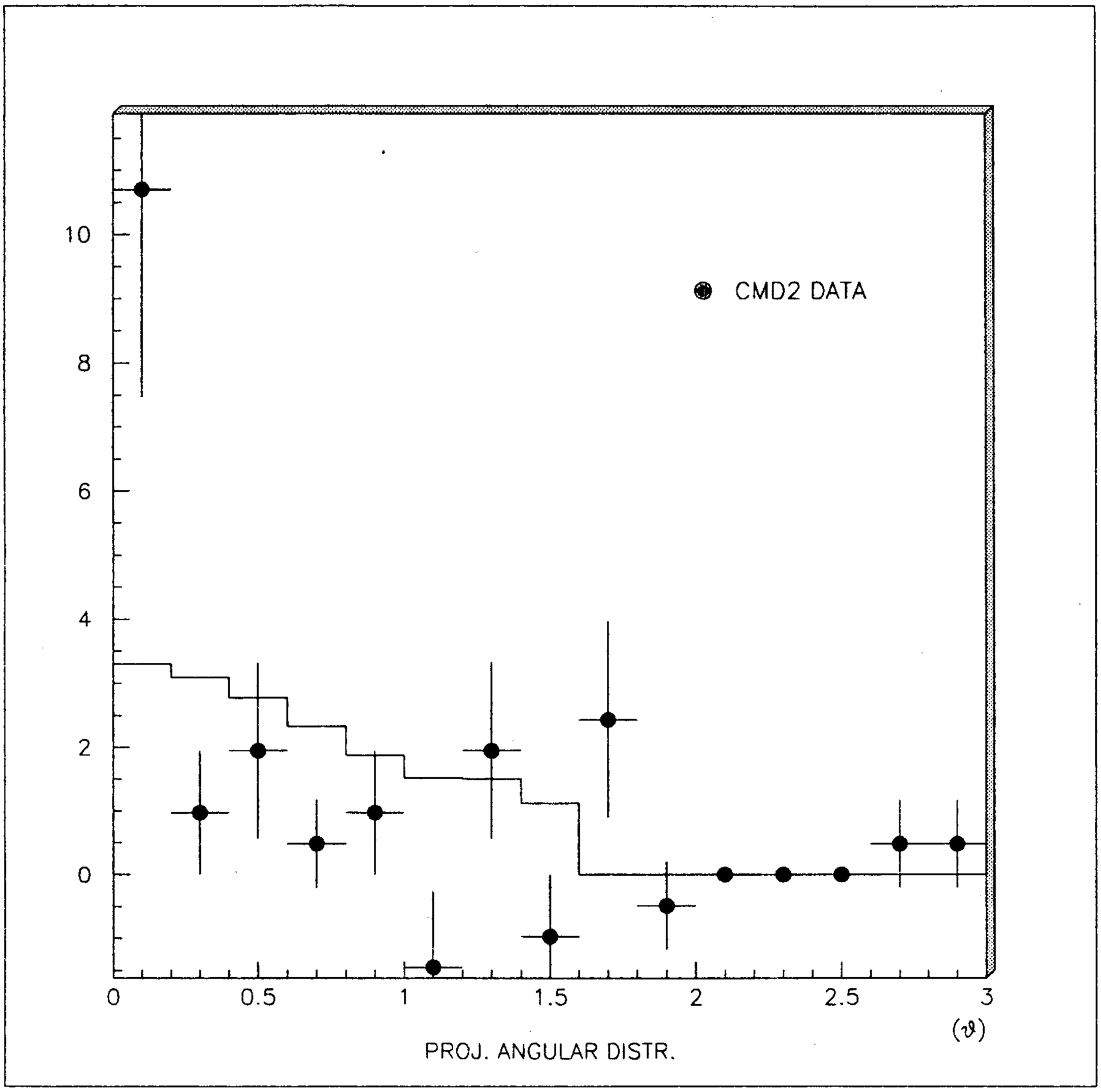

Figure 13: Comparison between projected regeneration angular distribution on Be from CMD2 data and E.A. predictions

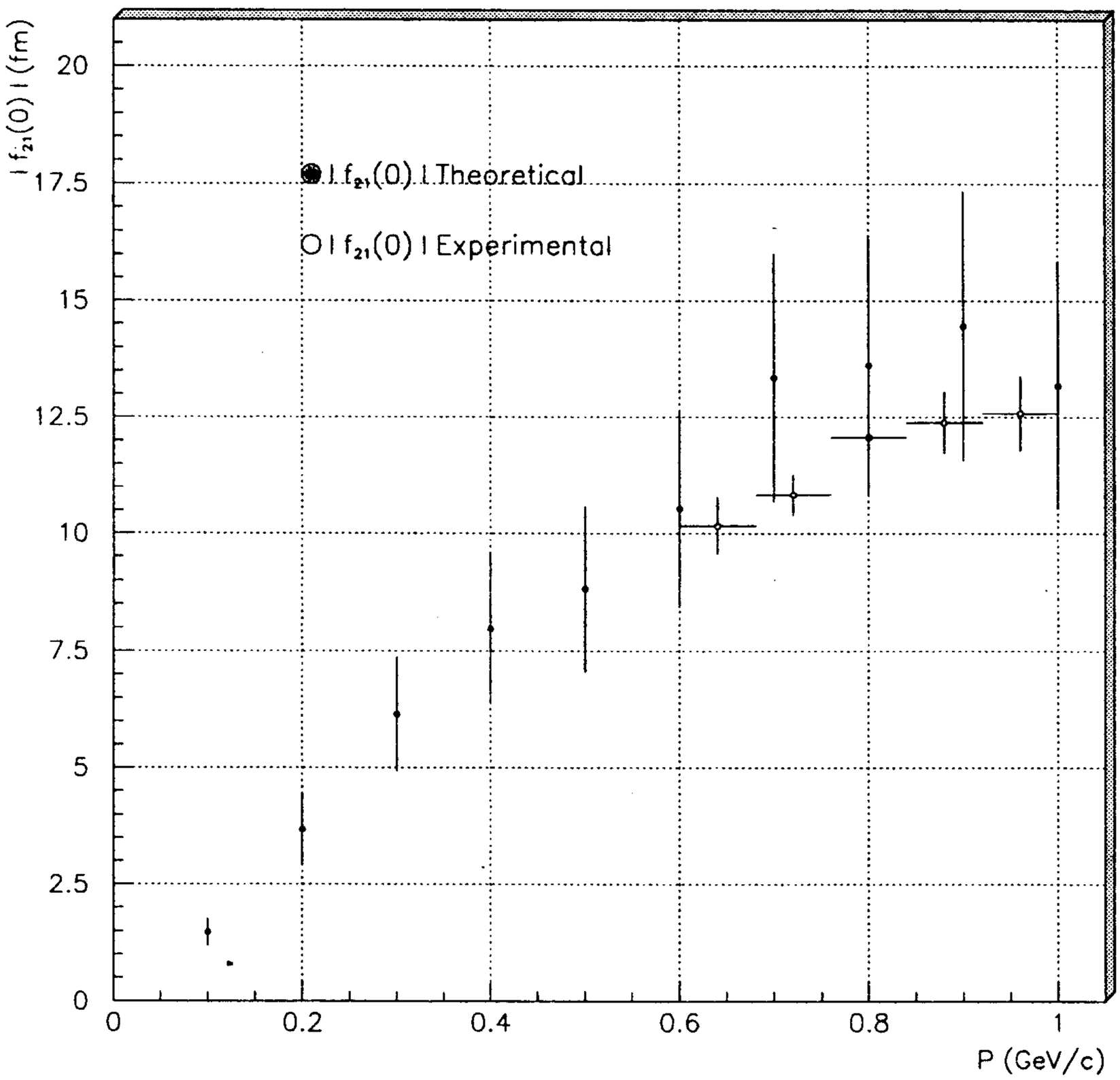

Figure 14: Experimental and theoretical forward regeneration amplitude on Cu.

around the K_L impinging direction . The statistical uncertainties is quite large ($\sim$ 20 events). Therefore only the qualitative conclusion of a fair agreement can be drawn.
Unfortunately the regeneration cross sections change abruptly just at K_L momenta $\simeq$ 100 $\div$ 200 MeV/c, depending on the atomic number of the nucleus, as shown in fig. 15$\div$17.
A strong cancellation is expected, in the imaginary parts at least, between K^+ and K^- elastic amplitudes. However at low momenta the K^-N elastic cross section grows, eventually diverging at threshold, and it is much larger than the K^+N elastic cross section. On this basis, it should be expected $\sigma_{reg} \approx \sigma_{el}$ at low momenta: for instance σ_{reg} on Be should be 260 mb, to be compared with the CMD2 measurment [16] and the E.A. prediction.
On the other hand, a large K^-N cross section introduces a screen for further K^-N interactions on a nucleus A and the K_LA elastic cross section, is expected to vary as $A^{2/3}$. Conversely for the K^+A elastic cross section, it is expected to vary as $A^2 \cdot \overline{F^2(k)}$, where $\overline{F^2(k)}$ is the nucleus form factor squared, averaged over the nucleus recoil momentum k. Therefore it can be foreseen qualitatively, that at low momenta and large atomic numbers A, the two elastic amplitudes cancel out in the regeneration amplitude.
The K^+ A elastic cross section evaluation at low momenta is the most controversial part for obtaining the regeneration cross section. A further check can be done for the imaginary part of the K^+ A forward elastic amplitude, using the experimental data of the total cross sections for K_L and K^-. The results are shown in table 11 : the agreement is fairly good and there is no experimental evidence for a smaller K^+ A amplitude at low momenta. Nevertheless the regeneration cross section, as obtained in this note, is so unexpected that it cannot be fully trusted without further checks, hopefully by means of other experimental data.

7.1 K_S regeneration on the beam pipe

K_S regeneration by a K_L beam traversing a slab may occur at various level of coherence on the nuclei of the slab. When the target is many nucleons of many nuclei, it is defined as "coherent" regeneration. Coherent regeneration is strictly forward. When the target is many nucleons of a single nucleus, it is defined as "diffractive" regeneration.
The ratio R between coherent and diffractive regeneration is independent of the regeneration cross section on a nucleus, but depends on the K_L momentum k and on the slab thickness

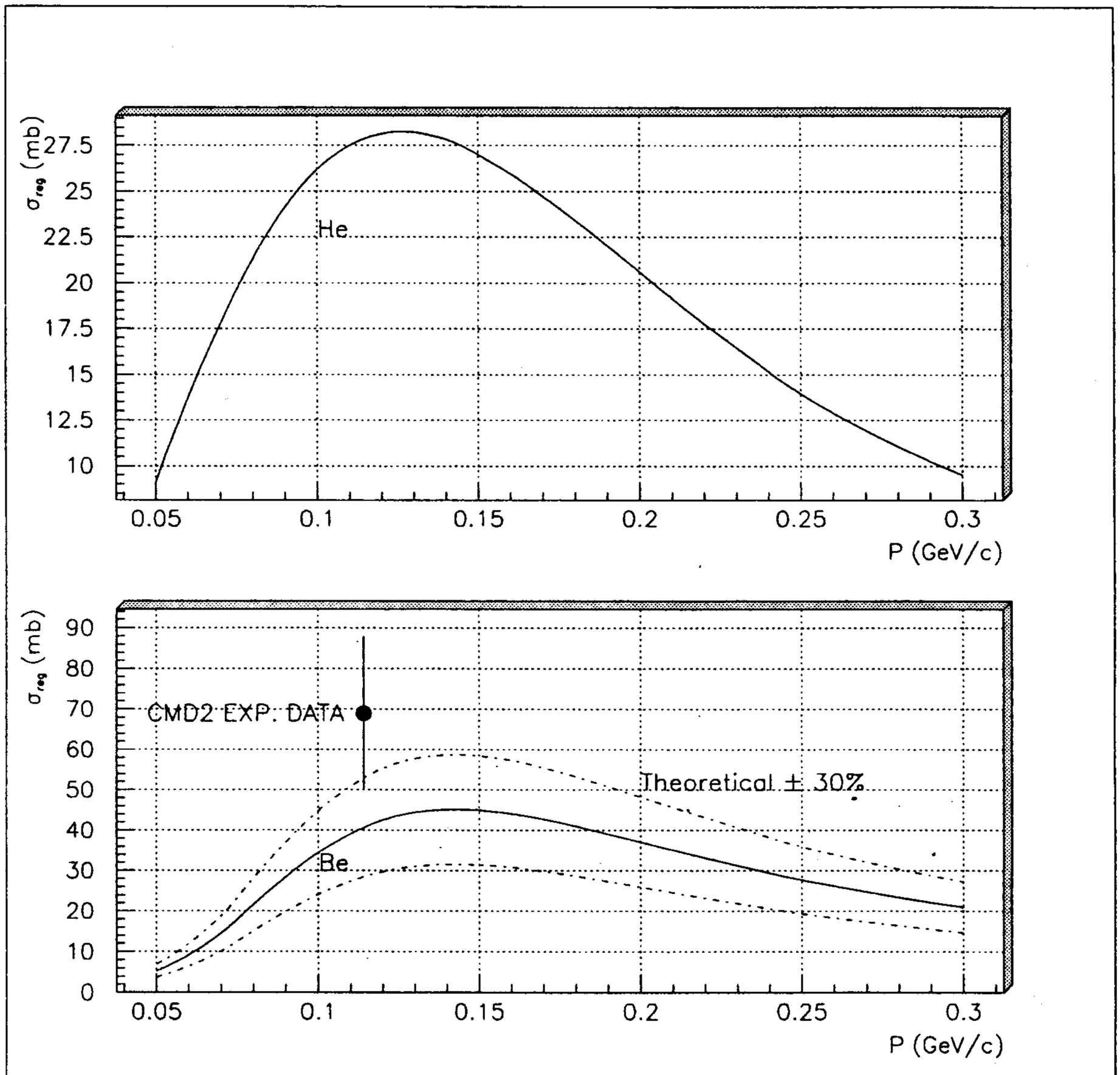

Figure 15: Regeneration cross section for He and Be comparing CMD2 data with theoretical predicitons.

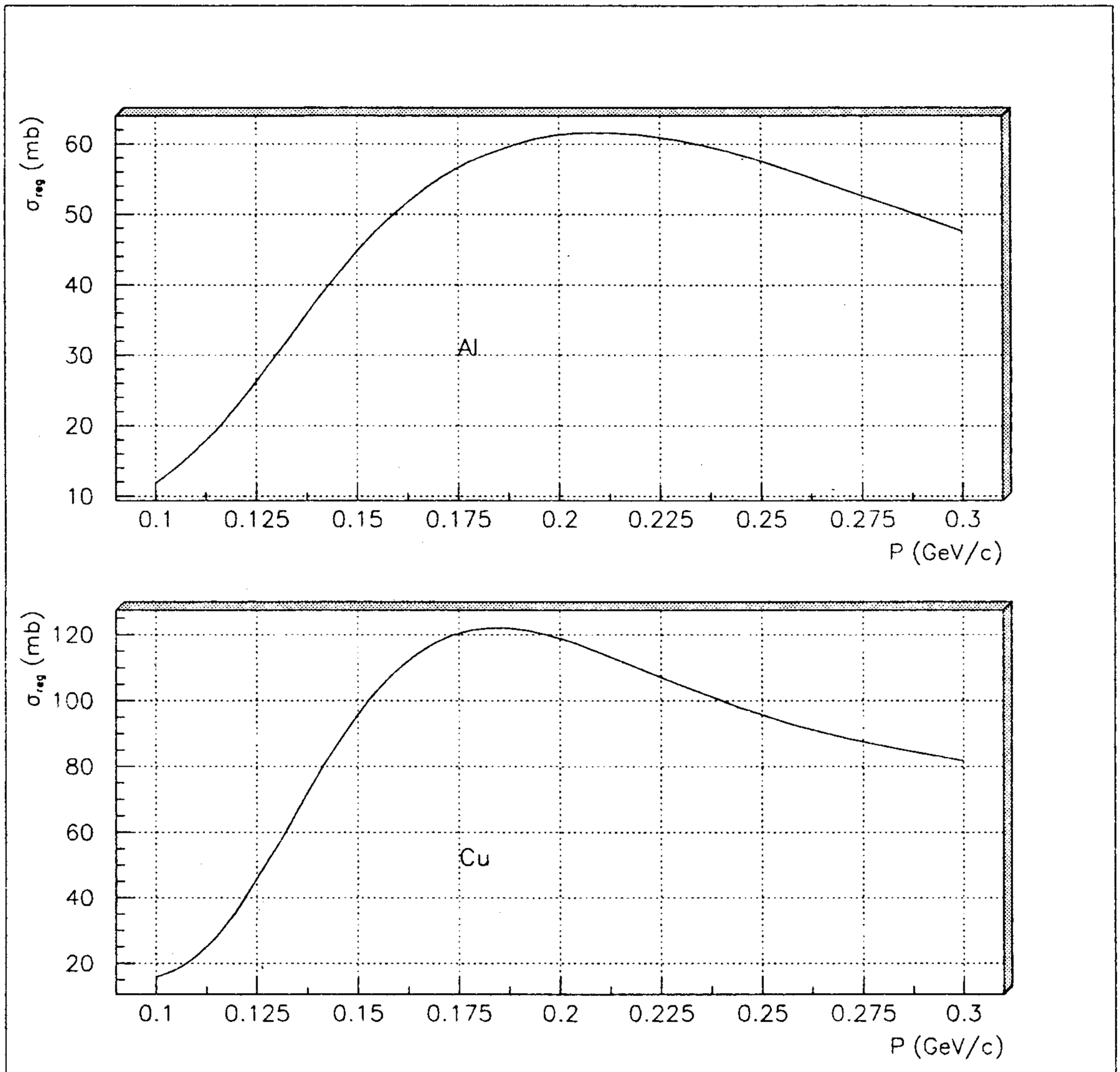

Figure 16: Regeneration cross section for Al and Cu.

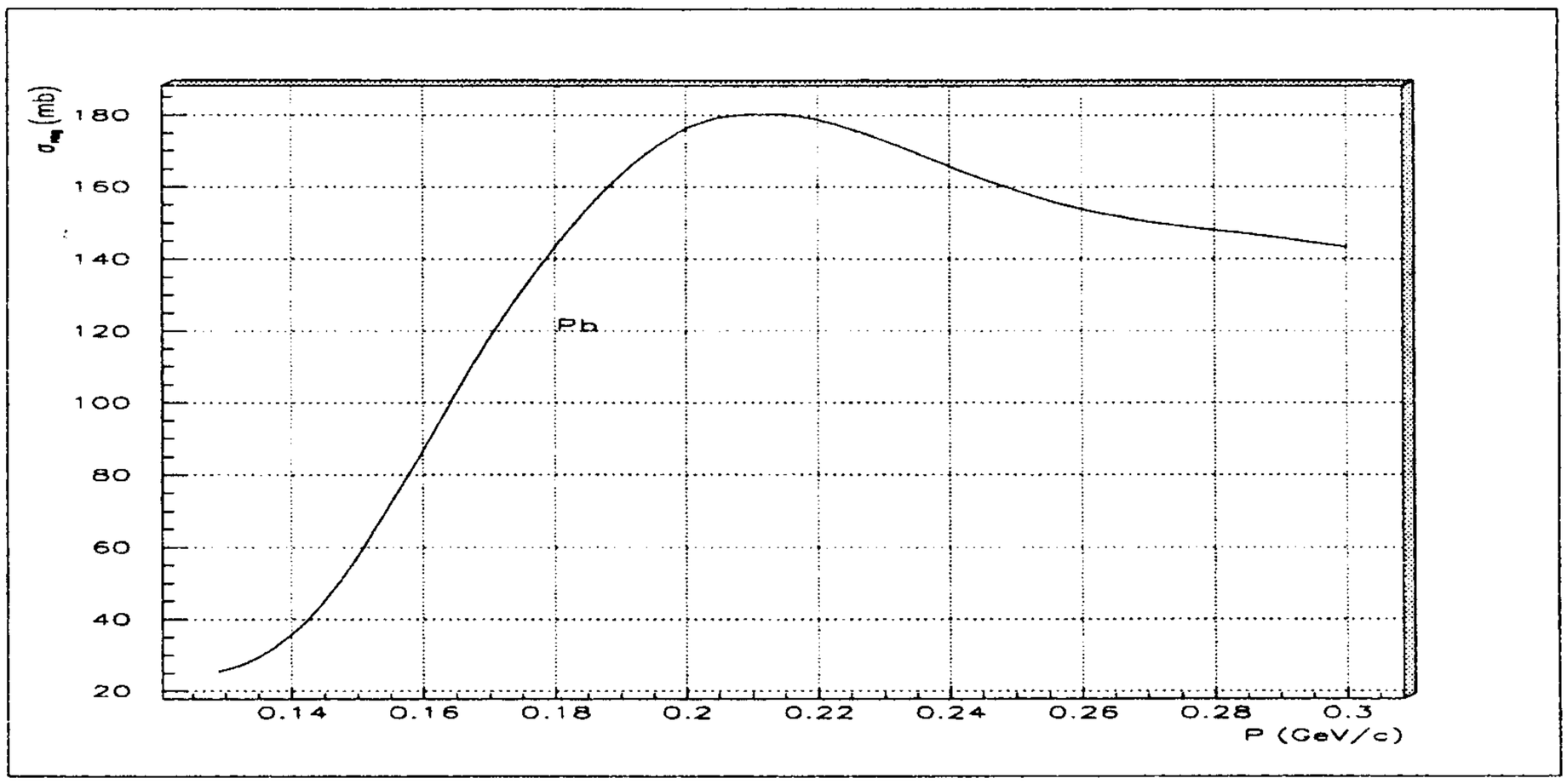

Figure 17: Regeneration cross section for Pb.

P (MeV/c)	Be (fm)	Be (fm)	C (fm)	C (fm)	Al (fm)	Al (fm)	Cu (fm)	Cu (fm)	Pb (fm)	Pb (fm)
50	1.4	3.0±0.5	1.6	3.5±0.4	2.4	4.8±2.3	4.0	6.7±2.7	8.2	13.1±5.4
100	1.9	2.3±0.7	2.5	2.7±0.6	4.1	4.5±1.6	6.8	5.9±3.2	15.6	16.6±6.7
150	1.7	1.9±0.8	2.3	2.4±0.7	5.3	4.6±1.8	10.9	5.7±3.7	20.3	20.9±8.0
200	1.6	1.7±0.9	2.2	2.3±0.8	5.5	5.2±2.1	12.8	5.9±4.2	29.7	25.9±9.3
250	1.6	1.7±1.0	2.1	2.4±0.8	5.5	5.9±2.3	13.3	6.6±4.7	36.8	31.4±10.6
300	1.6	1.9±1.0	2.1	2.6±0.9	5.4	7.0±2.6	13.5	7.6±5.2	41.0	37.5±11.9
350	1.6	1.9±1.1	2.1	2.9±1.0	5.2	7.9±2.8	12.9	8.3±5.7	41.4	42.7±13.2
400	1.9	1.6±1.2	2.4	2.7±1.0	5.6	8.4±3.0	13.6	8.7±6.2	43.3	47.8±14.5

Table 11: Comparison between Im f(0) obtained using E.A. (column without error) and from a mixture of experimental (K_L) and theoretical values (K^-).

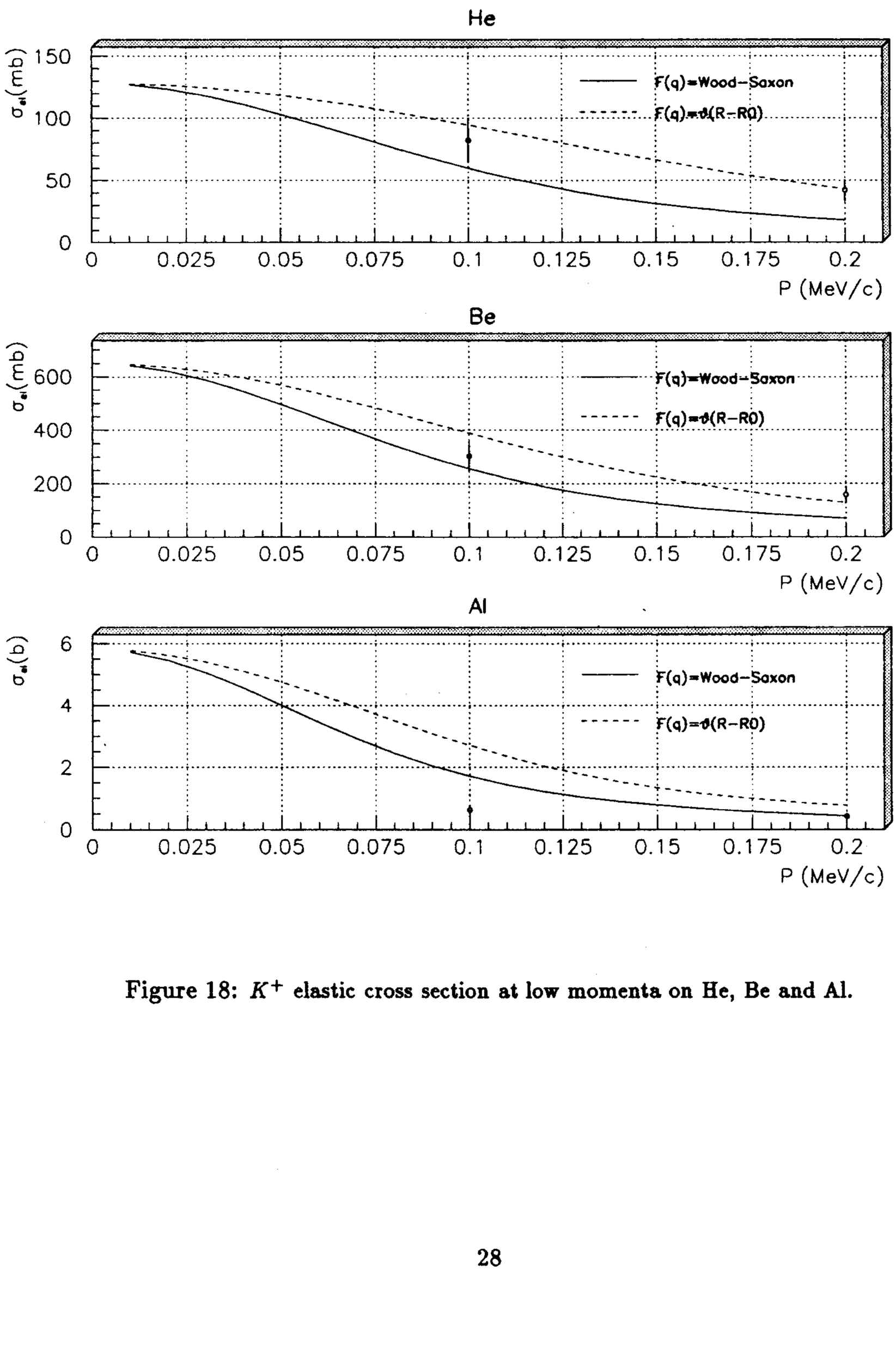

Figure 18: K^+ elastic cross section at low momenta on He, Be and Al.

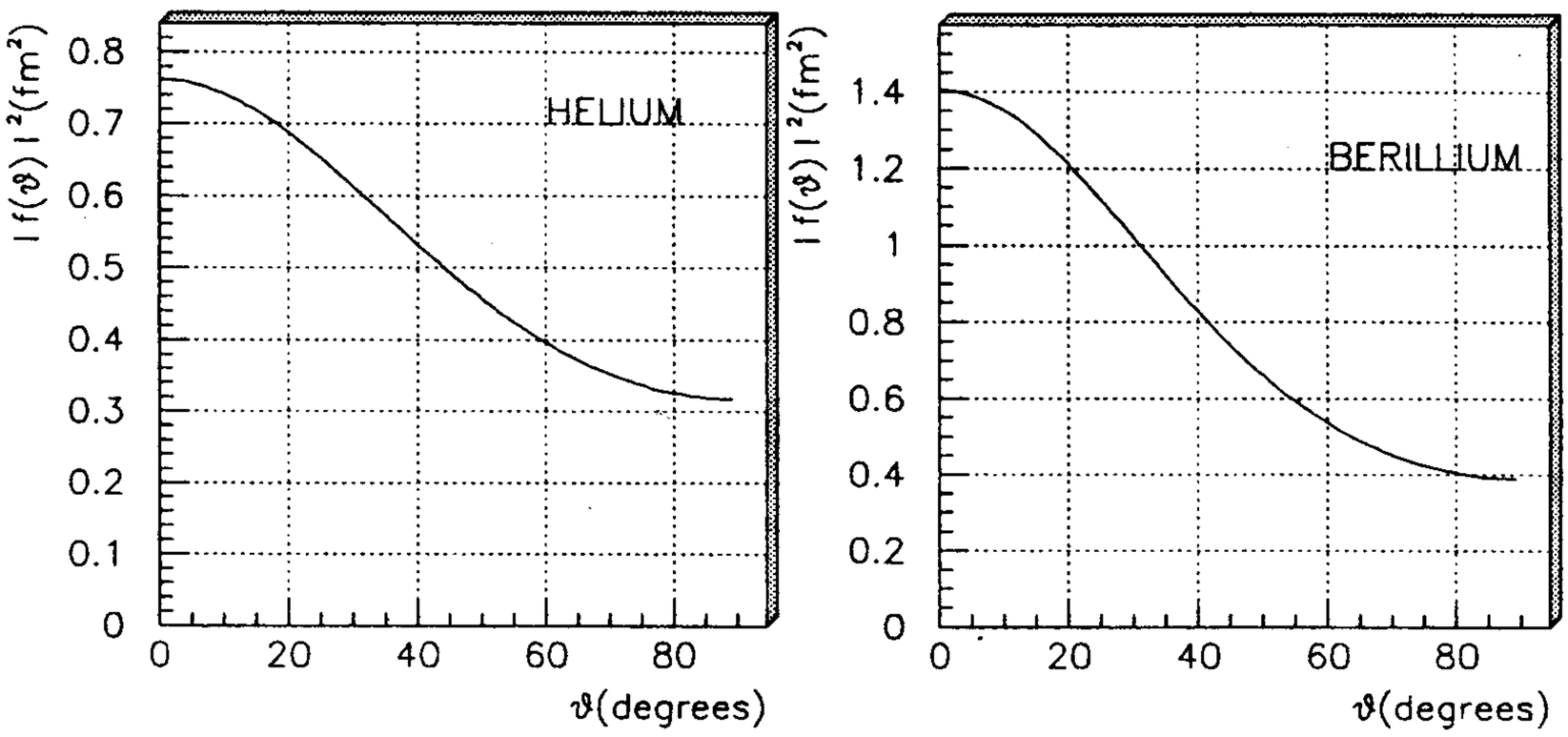

Figure 19: Regeneration angular distribution at $P = 114$ MeV/c for "light" nuclei.

Nucleus	Thickness (cm)	$\sigma^{coe}/\sigma^{diff}$
He	200	$4.1 \cdot 10^{-5}$
Be	0.05	$1.4 \cdot 10^{-2}$
Al	0.01	$1.4 \cdot 10^{-3}$

Table 12: Ratio between coherent and diffractive regeneration P=114 MeV/c.

L and density ρ [12]:

$$R = \frac{16\pi^2 \rho \tau_s |e^{-i\delta l} - e^{-l/2}|^2}{k\, m_k\, (1 - e^{-l})(1 + 4\delta^2)}$$

where

$$\delta = (m_L - m_S) \cdot \tau_S$$

$$l = L \cdot m_K / k$$

At low momenta the coherent contribution becomes more relevant. Ratios R in cases interesting for KLOE are shown in table 12. Coherent regeneration can be neglected in KLOE excepting the beam pipe regeneration from.

The DAΦNE beam-pipe in the KLOE interaction region has a complex shape. The radius of the beam pipe (500 μm Be thick) has been designed as large as possible ($\sim$ 10 cm) to avoid any complications arising from regeneration in the space region close to the interaction point. In fact quantum mechanics predicts, in the case the two Kaons decay in the same channel, an interference pattern, a few cm wide, in the relative distribution of two decay vertices (fig. 20). On the other hand DAΦNE's beam pipe has $\sim$ 3 cm radius and any discontinuity will act as a resonant parasitic cavity, which introduces an instability and an unwanted power dissipation in the storage ring operation. Therefore a very thin inner tube (60 μ Be thick at $r_T \sim$ 3 cm radius) will be inserted to avoid these drawbacks due to the KLOE requirement for a large beam pipe. Implications of a residual K_S regeneration from this thin tube with respect to the interference pattern have to be considered. However any regeneration contribution will be symmetric in the interference pattern. Calculations concerning the regeneration on the KLOE beam pipe are detailed in ref. [17].

Coherent regeneration is important, due to the interference with the K_S component from the Φ decay, still present at these distances. The inner tube is symmetric with respect to

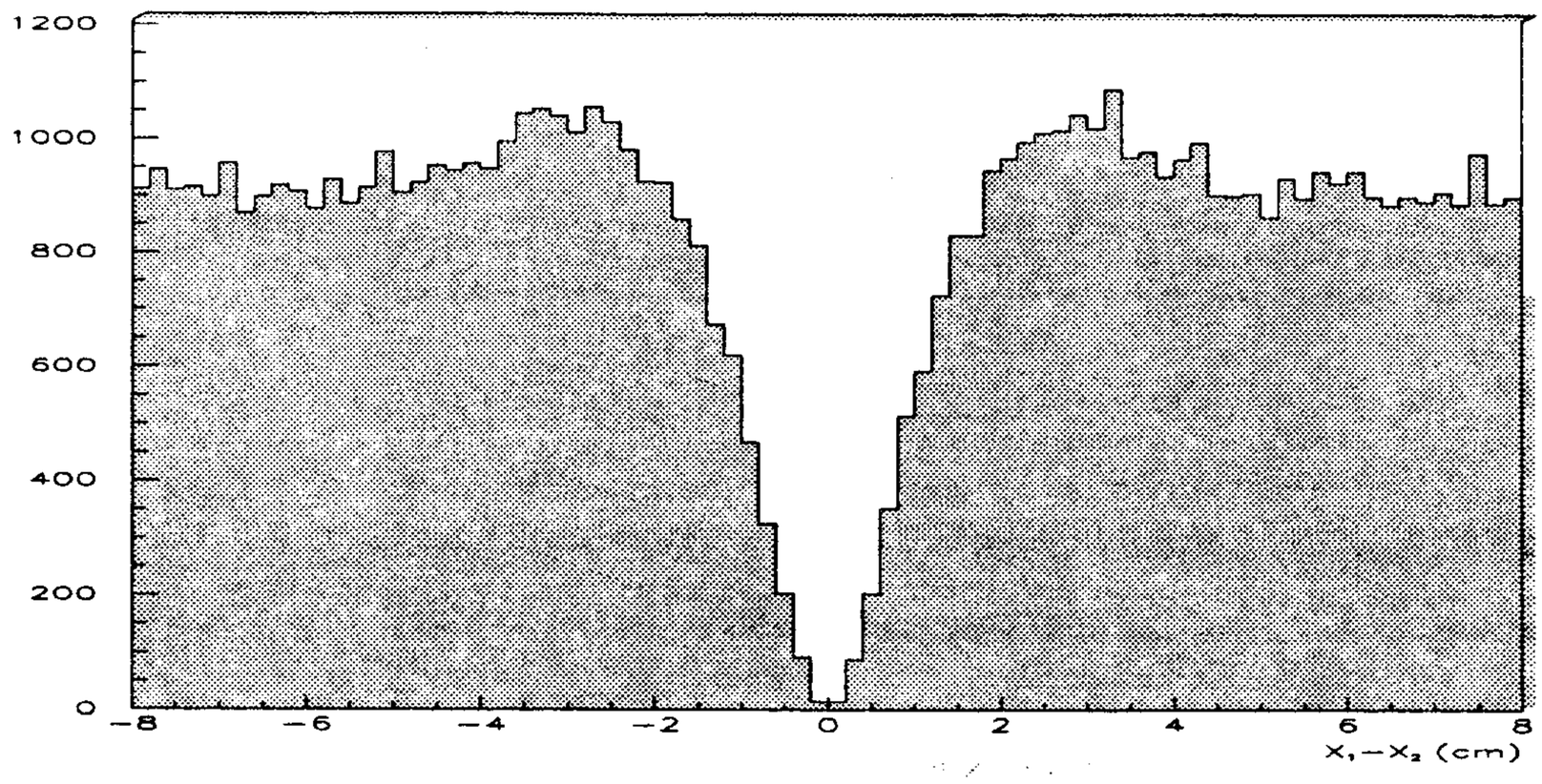

Figure 20: Interference pattern (ϵ'/ϵ=0).

the interaction region. Hence according to quantum mechanics any coherent regeneration contribution must vanish, if both the decay vertices will be outside (or inside) the inner tube [18]. In fact, taking into account coherent regeneration on both symmetric sides means making the substitutions:

$$K_L(\pm p) \rightarrow K_L(\pm p) + \alpha K_S(\pm p)$$

$$K_S(\pm p) \rightarrow K_S(\pm p) + \beta K_L(\pm p)$$

On the other hand the Φ wave function has to be antisymmetric (Bose-Einstein statistics,C conservation in a strong decay):

$$|\Phi >= \frac{1}{\sqrt{2}}[|K_S(p) > |K_L(-p) > -|K_S(-p) > |K_L(p) >]$$

so that, also after a coherent regeneration, any additional contribution $K_S K_S$ or $K_L K_L$ cancel out. Therefore coherent regeneration on one side only has to be considered, with an amplitude

$$a \doteq \imath \frac{2\pi}{k} N \cdot x \cdot f_{reg}(0)$$

where N is the Avogadro number and x is the thickness of the slab. On Be (50μ thick and

according to the regeneration amplitude reported in appendix) the amplitude modulus is $|a| \sim 8 \cdot 10^{-5}$ and the amplitude phase is $\alpha \sim \pi/4$.
Considering the case interesting for the ϵ'/ϵ measurement, both kaons decaying into two pions, the time evolution of the Φ wave function is:

$$\begin{aligned}\Phi \quad \propto \quad & \sqrt{\frac{2}{3}} e^{i(\gamma_s t_1 + \gamma_L T)} \left\{ c_{00} e^{i\gamma_L (t_2 - T)} + \frac{a}{\sqrt{3}} e^{i\gamma_s (t_2 - T)} \right\} - \\ - \quad & c_{+-} e^{i(\gamma_L t_1 + \gamma_S T)} \left\{ \frac{1}{\sqrt{3}} e^{i\gamma_S (t_2 - T)} + a\, e^{i\gamma_L (t_2 - T)} \right\}\end{aligned}$$

where t_1 and t_2 are the decay proper times in two pions with amplitudes $c_{00} \simeq 3.2 \cdot 10^{-2} e^{i\pi/4}$, $c_{+-} \sim \sqrt{2} c_{00}$ and $T = r_T / v_k$. Hence, coherent regeneration at the first order in a and c, neglecting Γ_L and ϵ'/ϵ, is:

$$\begin{aligned}\frac{1}{\frac{2}{3}|c_{00}|^2} |\Phi|^2 \quad \simeq & \, e^{-\Gamma_s t_1} + e^{-\Gamma_s t_2} - 2 e^{-\frac{\Gamma_s}{2}(t_1 + t_2)} \cos[\Delta m (t_2 - t_1)] + 2 \times \frac{1}{\sqrt{3}} \left| \frac{a}{c_{00}} \right| \\ & \left\{ e^{-\frac{\Gamma_s}{2}(2t_1 + t_2 - T)} \left[\cos\alpha \cos[\Delta m (t_2 - T)] + \sin\alpha \sin[\Delta m (t_2 - T)] \right] - \right. \\ & \left. - e^{-\frac{\Gamma_s}{2}(2t_2 + t_1 - T)} \left[\cos\alpha \cos[\Delta m (t_1 - T)] + \sin\alpha \sin[\Delta m (t_1 - T)] \right] \right\}\end{aligned}$$

In the case of diffractive regeneration there is no interference with the Φ wave function and, neglecting elastic diffractive scattering after the $\mathcal{CP}$ violation decay:

$$\frac{1}{\frac{2}{3}|c_{00}|^2} |\Delta\Phi|^2 = \frac{P_{reg}}{3|c_{00}|^2} e^{-\Gamma_S t_1} e^{-\Gamma_S (t_2 - T)}$$

In fig. 21 the asymmetry due to $\mathrm{Re}(\epsilon'/\epsilon) \sim 10^{-3}$ and in fig. 24 the effect of an imaginary part Im (ϵ'/ϵ)corresponding to a 1 degree phase are shown. For comparison in fig. 22 and in fig. 23 the contributions due to coherent and diffractive regeneration are set forth.

8 GEANT codes and K_L interactions in KLOE

In tables 13 and 14 the K_L total cross sections on various nuclei are shown, as obtained according the standard GEANT codes, GHEISHA and FLUKA.
In the GHEISHA package there is a warning that these cross sections cannot be trusted for K_L momenta lower than 2 GeV/c. Nevertheless variation from data in tables is impressive (a factor of $3 \div 10$, depending on the atomic number).

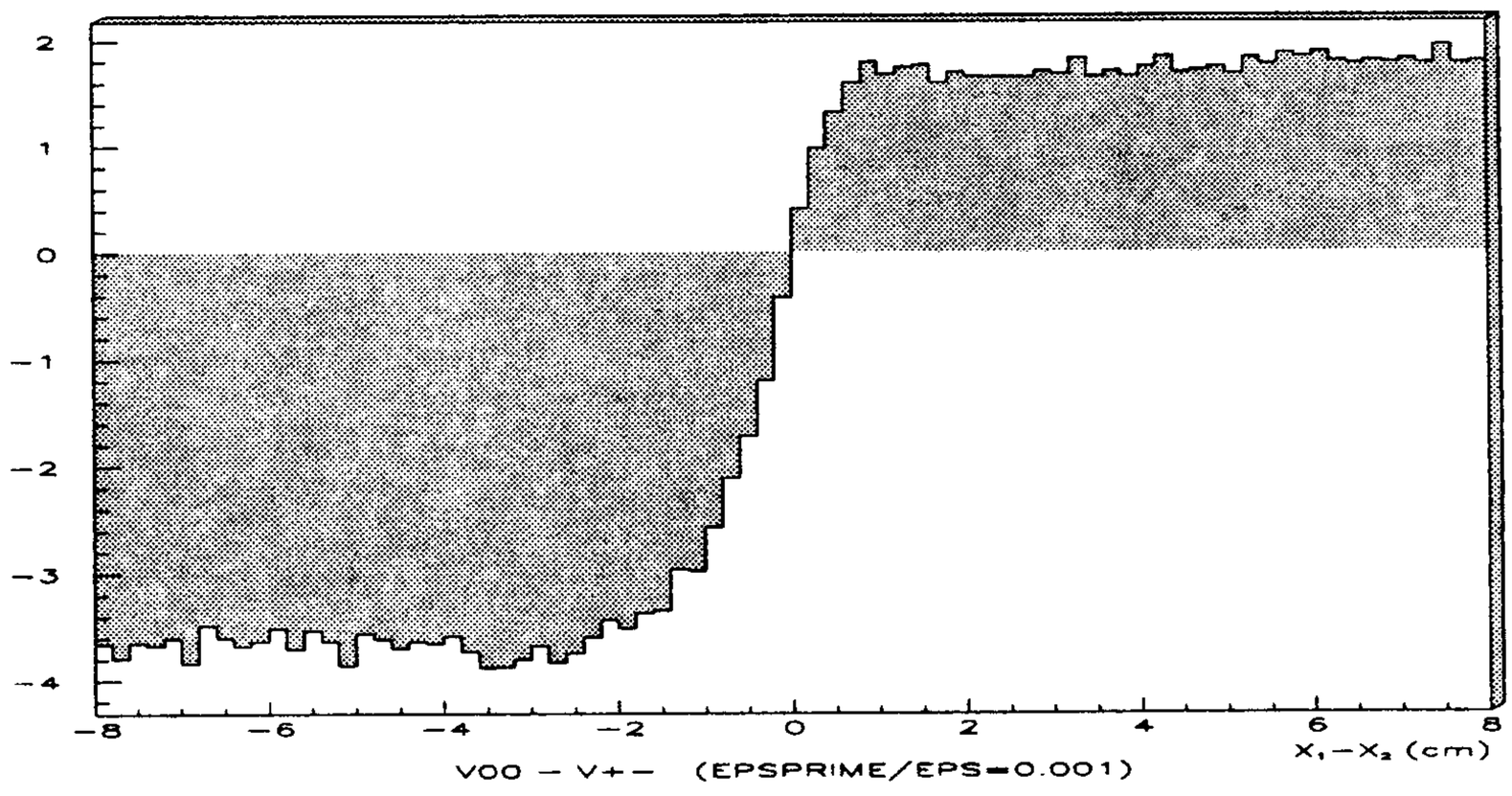

Figure 21: Asimmetry introduced in the intereference pattern by $\mathrm{Re}(\epsilon'/\epsilon \sim 10^{-3})$.

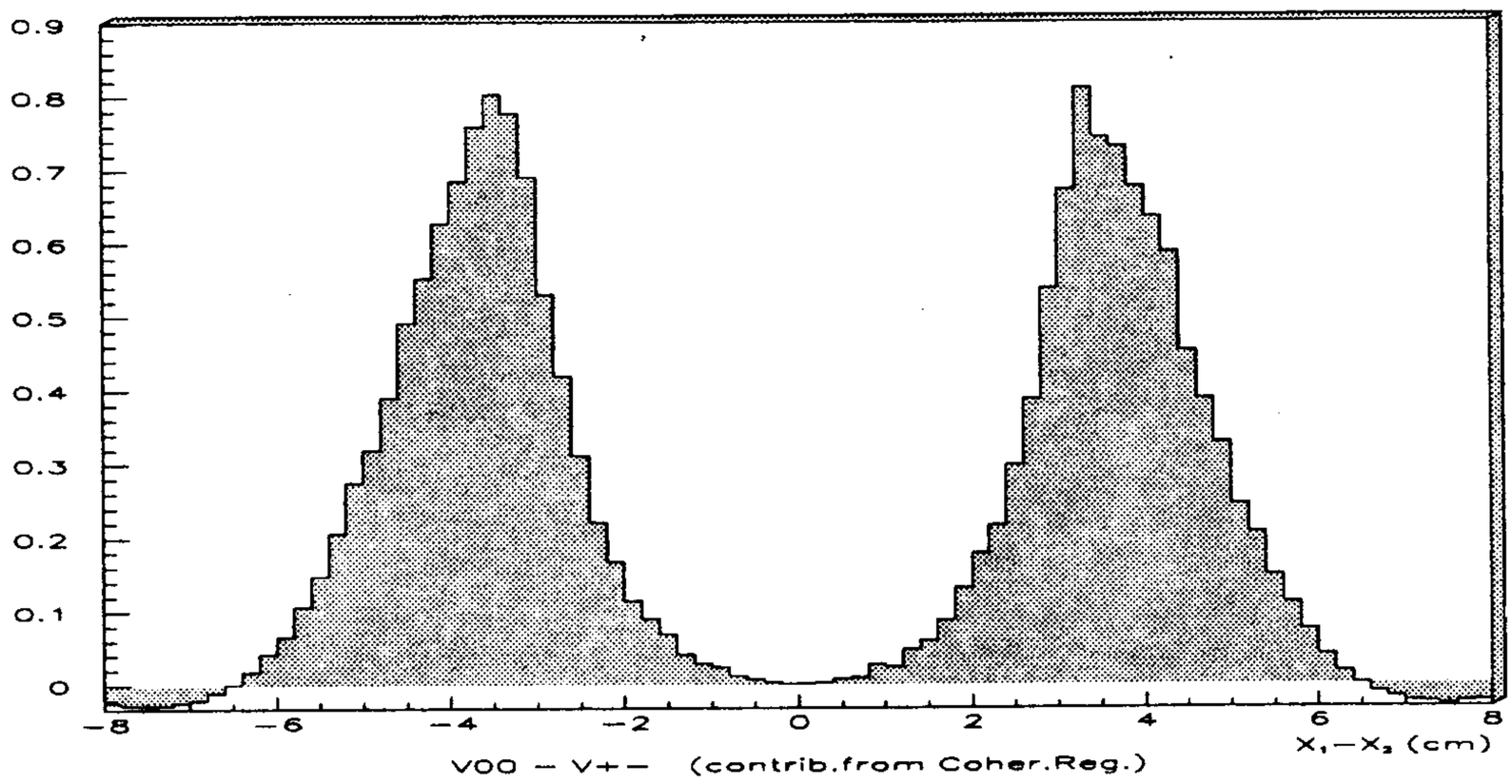

Figure 22: Coherent contribution to interference pattern.

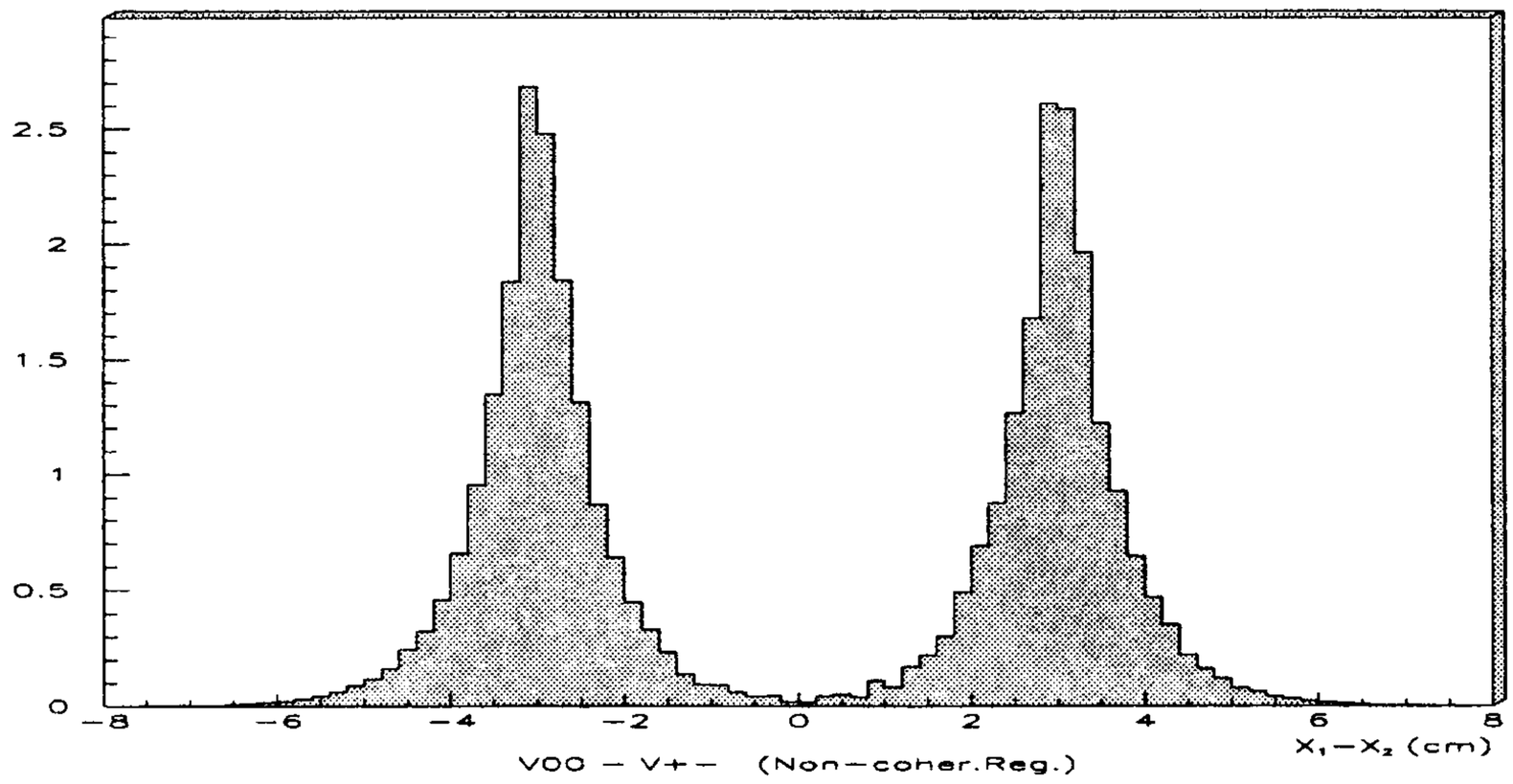

Figure 23: Diffraction regeneration contribution to the interference pattern.

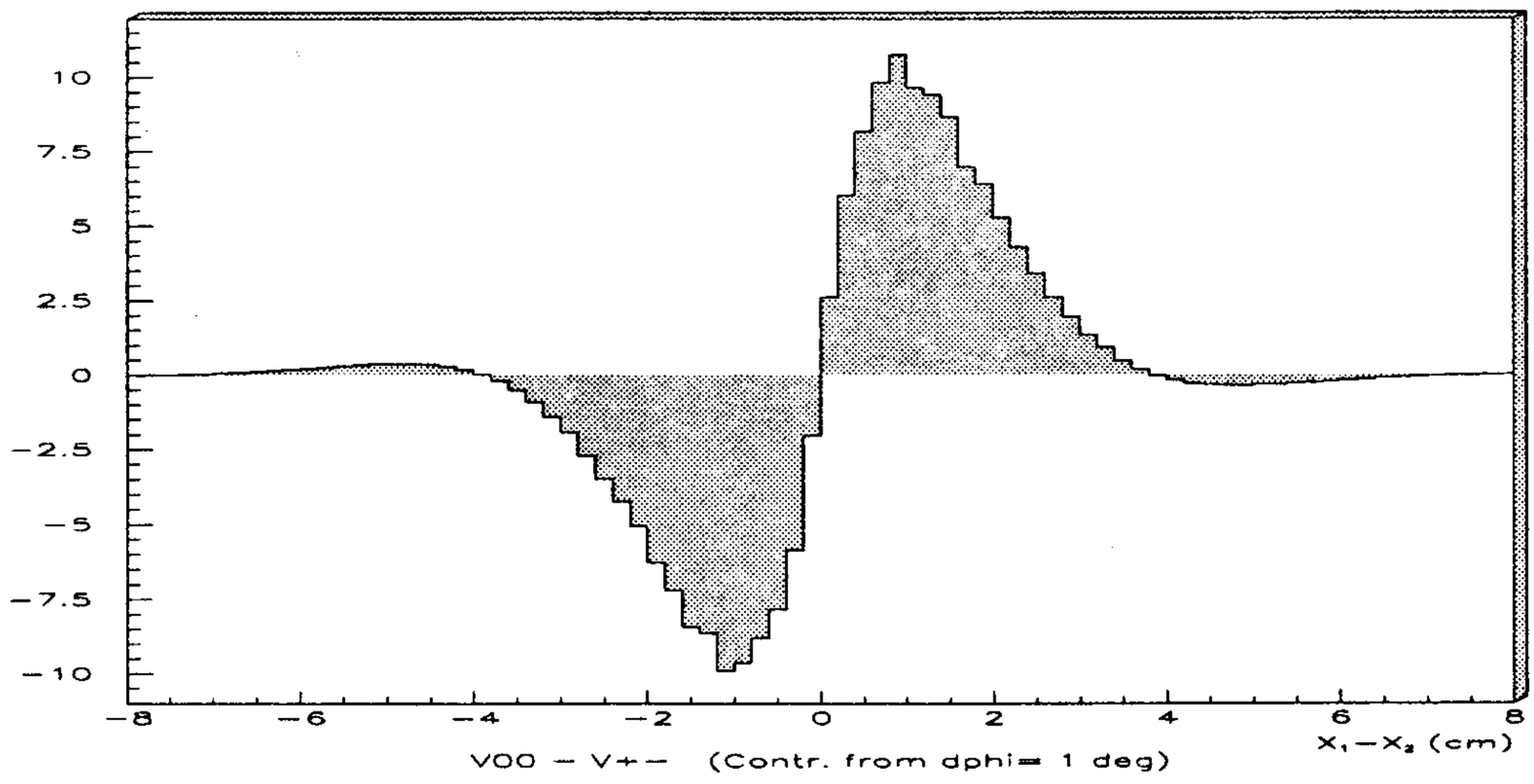

Figure 24: Contribution to the interference pattern of an imaginary part corresponding to 1° and $|\frac{\epsilon'}{\epsilon}| = 10^{-3}$.

P Mev/c	H (b)	Be (b)	C (b)	Al (b)	Fe (b)	Cu (b)	Pb (b)
168	0.17	1.7	2.4	5.0	10.5	10.9	36.1
177	0.16	1.6	2.2	4.8	10.1	10.1	32.4
187	0.15	1.6	2.1	4.3	8.8	9.6	29.6
197	0.14	1.5	1.8	3.8	7.8	8.8	27.6
209	0.14	1.3	1.6	3.3	6.6	7.2	23.5
223	0.13	1.0	1.4	2.7	5.4	5.9	19.3
239	0.12	0.9	1.1	2.5	4.2	4.7	14.5
258	0.11	0.8	1.0	1.9	3.7	4.1	12.2
281	0.10	0.7	0.9	1.7	3.2	3.8	10.8
308	0.08	0.6	0.8	1.6	3.0	3.3	9.8
343	0.08	0.5	0.7	1.4	2.9	3.2	9.7

Table 13: Cross section from GEANT simulation for K_L using GHEISHA package.

P Mev/c	H (mb)	Be (b)	C (b)	Al (b)	Fe (b)	Cu (b)	Pb (b)
168	0.0	0.0	0.0	0.0	0.0	0.0	0.0
177	0.0	0.0	0.0	0.0	0.0	0.0	0.0
187	0.0	0.0	0.0	0.0	0.0	0.0	0.0
197	0.0	0.0	0.0	0.0	0.0	0.0	0.0
209	0.0	0.0	0.0	0.0	0.0	0.0	0.0
223	0.0	0.0	0.0	0.0	0.0	0.0	0.0
239	25	0.3	0.3	0.7	1.1	1.3	3.2
258	23	0.3	0.3	0.6	1.1	1.3	3.2
281	23	0.3	0.3	0.6	1.1	1.2	3.2
308	21	0.3	0.3	0.6	1.1	1.2	3.2
343	21	0.3	0.3	0.6	1.1	1.2	3.2

Table 14: Cross sections from GEANT simulation using FLUKA package.

Nucleus	Thickness (cm)	σ_{el} (mb)	P_{int}
He	200	81±16	$(4.32 \pm 0.86) \cdot 10^{-4}$
Be	0.05	261±52	$(1.61 \pm 0.32) \cdot 10^{-3}$
Al	0.01	670±130	$(4.03 \pm 0.81) \cdot 10^{-4}$

Table 15: Cross section and interaction probability in KLOE.

In the case of the FLUKA package there is a much better agreement with the data, but unfortunately there are no inputs at low K_L momenta. On the other hand NUCRIN, the GHEISHA package for inelastic K_L interactions, is more realistic (that is, Λ and Σ are produced as expected).

In conclusion elastic and inelastic K_L interactions have been implemented in the KLOE MonteCarlo, GEANFI, according to the present note, both total and differential cross sections and according to NUCRIN, for the various inelastic interactions. Regeneration is a separate case.

K_L elastic scattering has to be taken into account if kinematical constraints between K_S and K_L are applied. In fact the two kaons are expected to be aligned, apart from a small boost due to the crossing angle of the incoming e^+e^- and due to radiation before their interaction. The probability for elastic scattering in the various KLOE materials are reported in table 15.

The interaction probability in the e.m. calorimeter has to be known for tagging the K_S by means of the K_L decaying or interacting.

Taking into account that the e.m. calorimeter is made of scintillating fiber, lead and glue in the ratio 42:42:10, the probability a K_L does not interact is:

$$P_0 = \exp[-(\sigma_{in}^{Pb} \cdot \rho_{Pb} \cdot l^{Pb} + \sigma_{in}^{C} \cdot \rho^{C} \cdot l^{C})] \sim 0.28$$

The probability that a K_L does not decay or interact in KLOE is

$$P^{dec} = \exp(-\frac{L_{ch} + L_{cal}}{L_{K_L} P_k / m_k}) \sim 0.12$$

By the way K_S decay events, if the K_L has not been detected, can be a background for $\gamma\gamma$ interaction identification $e^+e^- \rightarrow e^+e^-\pi\pi$citeZallo).

9 K_S regeneration inside the drift chamber

In the following the order of magnitude of the correction needed on the Re(ϵ'/ϵ) measurement, because of the K_S regeneration in the gas of the KLOE drift chamber, is estimated. A fiducial volume (R $\simeq$ 1.5 m radius) to detect K_L decay is defined in the KLOE drift chamber, filled with 90 % He and 10 % Isobutane. Most of the K_L are detected on a plane perpendicular to the beam axis (due to the $\sin^2\theta_k$ angular distribution).

According to the regeneration cross sections, the probabilities to have K_S regeneration due to the gas ($\delta_{gas} = 2.7 \times 10^{19}$ molecules/cm^3) of the KLOE drift chamber are given by:

$$\alpha_{He} \simeq \sigma_{He} \cdot \delta \cdot 0.9R \simeq 10^{-4}$$

$$\alpha_{C_4H_{10}} \simeq (4\sigma_C + 10\sigma_p) \cdot \delta \cdot 0.1R \simeq 1.2 \cdot 10^{-4}$$

The probability p to hit a wire, the amount l of K_L path through the wire and the probabilities α_w to have K_S regeneration due to the wires of the KLOE drift chamber are given by:

$$p = \frac{2N\rho}{\pi R}$$

$$l = \frac{\pi}{2}\rho$$

$$\alpha_w = (\sigma_{Al}N_{Al}\rho_{Al}^2 + \sigma_W N_W \rho_W^2)/R \simeq 0.4 \cdot 10^{-5}$$

where N_{Al} , N_W and ρ_{Al} , ρ_W are the total number and radii of Al and W wires inside the fiducial volume.

The K_S regeneration cross sections in the present calculation depend very strongly on their peculiar behaviour as a function of the kaon momentum. In the case of Be the calculation can be trusted, according to preliminary data from CMD2 [16] and according to the aforementioned data on He. An upper limit of the K_S regeneration cross sections on heavy elements, (like C , Al and W) can be obtained assuming:

$$\sigma_x \simeq \sigma_{Be} \cdot (A_x/A_{Be})^{2/3}$$

However the biggest contributions come from the regeneration on He and H, which are under control.

The expected angular distributions of the K_S regenerated on He, respect to the K_L flight direction, is shown in fig. 19 and that of K_S regenerated on proton are expected to be

rather flat. Hence a coplanarity cut on the angle between the decay plane and the K_L flight direction should be applied safely. In this way, looking for $\mathcal{CP}$ violation in the K_L decay, the contamination from regeneration events is strongly reduced: for instance a factor of 4 after a 30 degree cut can be achieved.

In conclusion the total regeneration probability α_{reg} in the KLOE drift chamber is

$$\alpha_{rej} \simeq 10^{-4}$$

times the probability the K_L does not decay before.

The number of events $K_L \to \pi^+\pi^-(N_{+-})$ and $K_L \to \pi^0\pi^0(N_{00})$ detected in the fiducial volume are related to α by:

$$N_{+-} \simeq N_L\,(1 - e^{R/x_L})\,[B^L_{+-} + \alpha\frac{X_L}{R}B^S_{+-}]$$

$$N_{00} \simeq N_L\,(1 - e^{R/x_L})\,[B^L_{00} + \alpha\frac{X_L}{R}B^S_{00}]$$

where N_L are the K_L crossing the fiducial volume, X_L the K_L mean free path, and B's are the K_L, K_S relative branching ratios into two pions. Therefore:

$$\mathrm{Re}(\frac{\epsilon'}{\epsilon})_{true} = \mathrm{Re}(\frac{\epsilon'}{\epsilon})_{exp}\left(1 + \alpha\frac{B^S_{00}\,X_L}{B^L_{00}\,R}\right)$$

In conclusion $\simeq$ 10 % enhancement is needed to estimate $\mathrm{Re}(\epsilon'/\epsilon)$, due to the expected contamination from K_S regeneration in the gas of the drift chamber. It is not crucial to have great accuracy for performing this correction. However few dedicated runs with additional concentrated regenerators will be enough to evaluate in detail this correction.

Acknowledgments

We warmly acknowledge Genia Solodov for many useful discussions and for the possibility to compare our calculations with the K_S regeneration on the CMD2 berillium beam pipe. We also acknowledge Juliet Lee Franzini for a careful review of this paper.

References

[1] The KLOE Collaboration, *The KLOE Detector Technical Proposal, LNF 93/002(IR).*

[2] Particle data Group (1994), *Physical review D50 (1994), 1173.*

[3] A.D.Martin, *Nucl. Phys. B179 (1981) 33.*

[4] J. K. Kim, *Ph.D thesis, Columbia U. (1966); NEVIS Report 149,1966.*

[5] R. H. Dalitz et al., *Proc. Int. Conf. on Hypernuclear and Kaon Physics, Heidelberg, 201 (1982).*

[6] J. E. Conboy, *Report RAL-85-091 (1985).*

[7] R.H.Dalitz, *Strange particles and strong interactions. (Oxford University Press, 1962)*

[8] G.A. Sayer e E.F. Beall, *Phys. Rev. 169 (1968) 1045.*

[9] W.Weise et al., *Il nuovo cimento Vol 102 A (1989) 265.*

[10] D. Birnbaum et al., *Phys. Rev. D9 (1974) 1242.*

[11] P. O. Mazur et al., *Phys. Rev. D Vol. 1 (1970) 20.*

[12] L.B. Okun, *Quarks e leptoni (Editori Riuniti, 1986).*

[13] Fey et al., *Z. Phys 265 (1973a) 401.*

[14] R.C. Barrett, D.F. Jackson, *Nuclear sizes and structure from p.154.*

[15] G. Alexander et al., *The KLOE small angle tagging system at DAFNE, Kloe note 112*

[16] R.R. Akhmetshin et al., *INP 95-62.*

[17] A. Michetti, *Studio delle interazioni dei Kaoni nel rivelatore KLOE, Tesi di laurea, 28 Maggio 1993.*

[18] R. Baldini et al., *Kaon Phisics at a Φ factory, LNF-90/007(R).*

Appendix: cross section tables

In this appendix K_L and charged Kaons cross sections are reported as obtained from the eikonal approximation for nuclei and from the A.D. Martin analisis for nucleon.

K_L p

P (GeV/c)	σ_{tot} (mb)	σ_{el} (mb)	σ_{an} (mb)	σ_{reg} (mb)	σ_{an}/σ_{el}	Re $f(0)$ (fm)	Im$f(0)$ (fm)
0.050	216.8	11.0	205.8	16.3	18.74	0.115	0.438
0.100	103.6	9.6	94.0	13.4	9.74	0.078	0.418
0.150	66.3	8.6	57.7	11.1	6.69	0.051	0.402
0.200	47.9	7.8	40.1	9.3	5.13	0.029	0.387
0.250	37.2	7.2	30.0	7.8	4.17	0.014	0.375
0.300	30.1	6.7	23.5	6.7	3.53	0.001	0.365
0.350	25.3	6.2	19.0	5.7	3.06	-0.008	0.357

K_L n

P (GeV/c)	σ_{tot} (mb)	σ_{el} (mb)	σ_{an} (mb)	σ_{reg} (mb)	σ_{an}/σ_{el}	Re $f(0)$ (fm)	Im$f(0)$ (fm)
0.050	291.3	39.8	251.6	17.7	6.33	-0.629	0.588
0.100	150.5	33.6	116.9	16.3	3.47	-0.512	0.608
0.150	98.0	28.2	69.7	14.1	2.47	-0.429	0.594
0.200	70.5	24.1	46.5	11.9	1.93	-0.373	0.570
0.250	54.1	20.9	33.2	10.0	1.59	-0.334	0.546
0.300	43.4	18.5	24.9	8.4	1.35	-0.307	0.526
0.350	36.0	16.6	19.4	7.2	1.16	-0.286	0.509

K_L He

P (GeV/c)	σ_{tot} (mb)	σ_{el} (mb)	σ_{an} (mb)	σ_{reg} (mb)	σ_{an}/σ_{el}	Re $f(0)$ (fm)	Im$f(0)$ (fm)
0.100	305.5	83.5	222.0	26.3	2.7	-0.61	1.23
0.114	277.1	80.9	196.2	27.9	2.4	-0.62	1.28
0.200	177.6	48.3	129.3	20.5	2.7	-0.62	1.43
0.300	123.1	21.7	101.5	9.5	4.7	-0.58	1.49
0.400	107.0	13.6	93.4	6.1	6.9	-0.34	1.73
0.500	87.3	8.7	78.5	3.6	9.0	-0.13	1.76
0.600	80.2	7.4	72.8	3.2	9.9	0.18	1.94
0.700	80.7	7.8	72.9	3.9	9.3	0.58	2.28
0.800	92.6	9.9	82.7	3.5	8.4	0.66	2.99
0.900	102.5	11.8	90.7	3.5	7.7	0.79	3.73
1.000	105.6	11.9	93.7	2.3	7.9	0.33	4.26

K_L Be

P (GeV/c)	σ_{tot} (mb)	σ_{el} (mb)	σ_{an} (mb)	σ_{reg} (mb)	σ_{an}/σ_{el}	Re $f(0)$ (fm)	Im$f(0)$ (fm)
0.100	596.6	267.6	329.0	34.7	1.2	-1.00	2.41
0.114	544.7	260.8	283.9	40.7	1.1	-1.10	2.51
0.200	357.8	144.6	213.2	37.1	1.5	-1.31	2.89
0.300	256.4	66.1	190.2	21.0	2.9	-1.30	3.11
0.400	227.2	44.8	182.4	15.9	4.1	-0.86	3.67
0.500	187.6	29.9	157.7	10.1	5.3	-0.45	3.79
0.600	174.0	25.5	148.5	9.4	5.8	0.16	4.22
0.700	175.0	26.5	148.5	11.2	5.6	0.89	4.95
0.800	195.6	31.8	163.8	9.7	5.2	1.02	6.32
0.900	212.3	36.6	175.8	9.3	4.8	1.22	7.72
1.000	217.3	36.9	180.4	6.3	4.9	0.48	8.78

K_L C

P (GeV/c)	σ_{tot} (mb)	σ_{el} (mb)	σ_{an} (mb)	σ_{reg} (mb)	σ_{an}/σ_{el}	Re $f(0)$ (fm)	Im$f(0)$ (fm)
0.100	725.5	362.2	363.3	36.2	1.0	-1.07	2.93
0.114	666.4	354.2	312.2	44.2	0.9	-1.20	3.07
0.200	443.7	190.6	253.1	43.8	1.3	-1.55	3.59
0.300	321.7	89.7	232.0	27.4	2.6	-1.57	3.90
0.400	280.3	60.3	220.0	19.8	3.6	-1.04	4.53
0.500	236.9	42.0	194.9	12.9	4.6	-0.53	4.78
0.600	222.2	36.9	185.4	12.1	5.0	0.24	5.39
0.700	226.3	39.2	187.1	14.7	4.8	1.12	6.40
0.800	251.4	46.4	205.0	12.5	4.4	1.24	8.12
0.900	272.4	53.0	219.4	11.9	4.1	1.46	9.90
1.000	275.8	52.5	223.3	7.6	4.3	0.53	11.14

K_L Al

P (GeV/c)	σ_{tot} (mb)	σ_{el} (mb)	σ_{an} (mb)	σ_{reg} (mb)	σ_{an}/σ_{el}	Re $f(0)$ (fm)	Im$f(0)$ (fm)
0.100	1148.2	634.5	513.7	11.9	0.8	-0.95	4.64
0.114	1115.6	667.1	448.6	18.6	0.7	-1.17	5.14
0.200	838.4	425.1	413.3	61.3	1.0	-2.37	6.77
0.300	626.9	238.9	388.0	47.6	1.6	-2.86	7.60
0.400	542.5	163.1	379.3	34.4	2.3	-2.19	8.77
0.500	469.3	120.8	348.5	24.9	2.9	-1.35	9.48
0.600	446.4	108.8	337.6	24.2	3.1	-0.10	10.82
0.700	454.8	113.9	341.0	28.9	3.0	1.21	12.86
0.800	488.7	125.1	363.6	22.9	2.9	1.34	15.79
0.900	517.7	135.8	381.9	20.6	2.8	1.64	18.82
1.000	520.3	133.6	386.7	13.4	2.9	0.41	21.02

K_L Fe

P (GeV/c)	σ_{tot} (mb)	σ_{el} (mb)	σ_{an} (mb)	σ_{reg} (mb)	σ_{an}/σ_{el}	Re $f(0)$ (fm)	Im$f(0)$ (fm)
0.100	1747.5	926.1	821.4	12.6	0.9	-1.08	7.06
0.114	1744.4	957.3	787.1	19.8	0.8	-1.17	8.03
0.200	1504.0	802.9	701.1	107.8	0.9	-3.28	12.15
0.300	1169.9	520.4	649.5	73.5	1.2	-4.79	14.18
0.400	1008.0	360.5	647.5	56.8	1.8	-4.10	16.29
0.500	883.8	275.1	608.6	43.1	2.2	-2.84	17.85
0.600	846.2	250.0	596.2	42.6	2.4	-0.87	20.51
0.700	859.5	257.9	601.6	50.2	2.3	1.00	24.30
0.800	903.8	272.8	631.0	38.6	2.3	1.21	29.21
0.900	943.4	288.6	654.9	33.7	2.3	1.65	34.30
1.000	945.1	284.0	661.1	22.1	2.3	0.06	38.18

K_L Cu

P (GeV/c)	σ_{tot} (mb)	σ_{el} (mb)	σ_{an} (mb)	σ_{reg} (mb)	σ_{an}/σ_{el}	Re $f(0)$ (fm)	Im$f(0)$ (fm)
0.100	1945.5	1007.5	938.0	15.9	0.9	-1.23	7.86
0.114	1940.3	1025.6	914.7	26.5	0.9	-1.29	8.93
0.200	1694.1	914.2	779.9	118.9	0.9	-3.59	13.69
0.300	1323.8	591.2	732.6	81.8	1.2	-5.36	16.04
0.400	1142.1	413.4	728.7	62.9	1.8	-4.65	18.45
0.500	1000.8	315.8	685.0	48.2	2.2	-3.27	20.21
0.600	957.7	286.6	671.0	47.8	2.3	-1.09	23.21
0.700	971.2	294.6	676.6	56.3	2.3	0.97	27.46
0.800	1019.3	310.4	708.9	43.3	2.3	1.23	32.94
0.900	1062.6	327.6	735.0	37.6	2.2	1.73	38.63
1.000	1065.0	322.7	742.3	24.8	2.3	0.00	43.02

K_L Pb

P (GeV/c)	σ_{tot} (mb)	σ_{el} (mb)	σ_{an} (mb)	σ_{reg} (mb)	σ_{an}/σ_{el}	Re $f(0)$ (fm)	Im$f(0)$ (fm)
0.100	4068.1	2021.0	2047.1	53.5	1.0	-2.19	16.43
0.114	3884.9	1829.4	2055.4	38.9	1.1	-2.66	17.89
0.200	3715.4	2043.9	1671.5	176.2	0.8	-2.90	30.02
0.300	3386.3	1775.0	1611.3	143.3	0.9	-8.30	41.04
0.400	2985.9	1354.5	1631.4	109.4	1.2	-10.03	48.25
0.500	2662.7	1086.8	1575.9	88.4	1.5	-8.88	53.78
0.600	2550.9	988.8	1562.1	88.6	1.6	-5.69	61.83
0.700	2542.3	974.5	1567.7	102.0	1.6	-3.24	71.89
0.800	2578.6	966.4	1612.2	76.2	1.7	-2.26	83.33
0.900	2628.4	979.9	1648.6	63.3	1.7	-0.98	95.56
1.000	2633.9	970.0	1663.8	43.4	1.7	-2.71	106.39

K^- p

P (GeV/c)	σ_{tot} (mb)	σ_{el} (mb)	σ_{an} (mb)	σ_{an}/σ_{el} (mb)	Re $f(0)$	Im$f(0)$ (fm)
0.050	569.0	101.2	467.7	4.62	-0.75	1.15
0.100	287.5	86.4	201.2	2.33	-0.52	1.16
0.150	182.6	71.3	111.3	1.56	-0.36	1.11
0.200	128.0	58.8	69.2	1.18	-0.26	1.03
0.250	95.4	49.0	46.4	0.95	-0.19	0.96
0.300	74.3	41.4	32.9	0.79	-0.14	0.90

K^- n

P (GeV/c)	σ_{tot} (mb)	σ_{el} (mb)	σ_{an} (mb)	σ_{an}/σ_{el} (mb)	Re $f(0)$ (fm)	Im$f(0)$ (fm)
0.050	426.7	51.5	375.2	7.29	0.47	0.86
0.100	200.4	43.0	157.4	3.66	0.39	0.81
0.150	125.9	36.5	89.4	2.45	0.33	0.76
0.200	89.3	31.3	58.0	1.85	0.29	0.72
0.250	67.9	27.2	40.7	1.49	0.25	0.69
0.300	54.0	23.9	30.1	1.26	0.23	0.66

K^- He

P (GeV/c)	σ_{tot} (mb)	σ_{el} (mb)	σ_{an} (mb)	σ_{an}/σ_{el} (mb)	Re $f(0)$ (fm)	Im$f(0)$ (fm)
0.100	450.7	137.2	313.5	2.3	-0.06	1.82
0.200	285.8	95.2	190.6	2.0	0.03	2.31
0.300	196.9	44.3	152.6	3.4	0.10	2.39
0.400	167.1	30.9	136.2	4.4	0.42	2.70
0.500	126.6	19.0	107.6	5.7	0.74	2.56
0.600	110.3	16.5	93.7	5.7	1.31	2.67
0.700	111.3	19.4	91.9	4.7	2.07	3.15
0.800	129.6	22.6	107.0	4.7	2.14	4.19
0.900	145.3	26.3	119.0	4.5	2.31	5.28
1.000	147.1	23.6	123.5	5.2	1.35	5.94

K^- Be

P (GeV/c)	σ_{tot} (mb)	σ_{el} (mb)	σ_{an} (mb)	σ_{an}/σ_{el} (mb)	Re $f(0)$ (fm)	Im$f(0)$ (fm)
0.100	727.0	302.4	424.6	1.4	-.12	2.94
0.200	514.2	205.8	308.4	1.5	-.03	4.15
0.300	380.4	110.1	270.3	2.5	0.09	4.61
0.400	339.6	89.5	250.1	2.8	0.69	5.49
0.500	264.4	58.7	205.7	3.5	1.32	5.34
0.600	235.8	52.5	183.3	3.5	2.43	5.72
0.700	240.2	60.7	179.5	3.0	3.82	6.79
0.800	271.8	68.4	203.4	3.0	3.84	8.78
0.900	296.9	76.4	220.4	2.9	4.04	10.79
1.000	298.6	69.8	228.8	3.3	2.46	12.06

K^- C

P (GeV/c)	σ_{tot} (mb)	σ_{el} (mb)	σ_{an} (mb)	σ_{an}/σ_{el} (mb)	Re $f(0)$ (fm)	Im$f(0)$ (fm)
0.100	844.1	378.2	465.8	1.2	-0.08	3.41
0.200	616.4	250.3	366.0	1.5	0.04	4.98
0.300	467.5	144.9	322.6	2.2	0.19	5.67
0.400	412.1	116.6	295.5	2.5	0.84	6.66
0.500	329.7	80.4	249.3	3.1	1.61	6.66
0.600	298.0	73.6	224.4	3.0	2.97	7.22
0.700	307.3	86.3	221.1	2.6	4.69	8.69
0.800	344.6	95.6	248.9	2.6	4.62	11.13
0.900	376.4	106.8	269.7	2.5	4.79	13.68
1.000	372.8	95.4	277.4	2.9	2.81	15.06

K^- Al

P (GeV/c)	σ_{tot} (mb)	σ_{el} (mb)	σ_{an} (mb)	σ_{an}/σ_{el} (mb)	Re $f(0)$ (fm)	Im$f(0)$ (fm)
0.100	1286.4	654.3	632.0	1.0	-0.12	5.20
0.200	995.6	402.0	593.6	1.5	0.02	8.04
0.300	805.2	295.7	509.5	1.7	0.21	9.76
0.400	735.8	253.1	482.6	1.9	1.14	11.89
0.500	618.1	195.2	422.9	2.2	2.40	12.48
0.600	577.3	187.2	390.1	2.1	4.59	13.99
0.700	601.6	216.3	385.3	1.8	7.12	17.01
0.800	649.8	227.5	422.3	1.9	6.76	21.00
0.900	691.2	242.6	448.6	1.8	6.79	25.13
1.000	678.5	219.3	459.2	2.1	4.07	27.41

K^- Fe

P (GeV/c)	σ_{tot} (mb)	σ_{el} (mb)	σ_{an} (mb)	σ_{an}/σ_{el}	Re $f(0)$ (fm)	Im$f(0)$ (fm)
0.100	1974.7	1030.8	943.9	0.9	-0.17	7.98
0.200	1615.1	705.2	909.9	1.3	-0.01	13.05
0.300	1368.4	544.3	824.1	1.5	0.24	16.58
0.400	1280.3	491.6	788.7	1.6	1.55	20.69
0.500	1113.1	401.2	711.9	1.8	3.54	22.48
0.600	1061.5	393.3	668.2	1.7	6.95	25.73
0.700	1109.7	448.3	661.4	1.5	10.59	31.38
0.800	1170.7	459.6	711.1	1.5	9.78	37.83
0.900	1224.0	478.9	745.1	1.6	9.61	44.50
1.000	1197.8	437.8	760.0	1.7	5.89	48.38

K^- Cu

P (GeV/c)	σ_{tot} (mb)	σ_{el} (mb)	σ_{an} (mb)	σ_{an}/σ_{el}	Re $f(0)$ (fm)	Im$f(0)$ (fm)
0.100	2205.6	1127.7	1078.0	1.0	-0.21	8.91
0.200	1808.2	798.4	1009.8	1.3	-0.03	14.61
0.300	1535.7	610.9	924.9	1.5	0.23	18.61
0.400	1441.5	555.3	886.2	1.6	1.70	23.29
0.500	1254.9	455.2	799.6	1.8	3.91	25.35
0.600	1197.9	446.7	751.2	1.7	7.70	29.03
0.700	1251.3	507.9	743.4	1.5	11.72	35.38
0.800	1318.2	520.1	798.1	1.5	10.82	42.60
0.900	1375.9	540.7	835.2	1.5	10.63	50.02
1.000	1347.8	495.7	852.1	1.7	6.55	54.44

K^- Pb

P (GeV/c)	σ_{tot} (mb)	σ_{el} (mb)	σ_{an} (mb)	σ_{an}/σ_{el}	Re $f(0)$ (fm)	Im$f(0)$ (fm)
0.100	4273.3	1947.4	2325.9	1.2	-0.39	17.26
0.200	3756.5	1719.3	2037.1	1.2	-0.23	30.35
0.300	3393.3	1497.5	1895.8	1.3	0.07	41.12
0.400	3291.8	1429.9	1861.9	1.3	2.21	53.19
0.500	3018.2	1273.3	1744.8	1.4	5.77	60.96
0.600	2959.2	1278.7	1680.5	1.3	11.84	71.72
0.700	3065.2	1395.5	1669.7	1.2	17.28	86.67
0.800	3130.6	1385.0	1745.6	1.3	15.54	101.17
0.900	3191.1	1396.7	1794.4	1.3	15.02	116.01
1.000	3143.6	1319.7	1823.9	1.4	9.84	126.99

K^+ p

P (GeV/c)	σ_{tot} (mb)	σ_{el} (mb)	σ_{an} (mb)	σ_{an}/σ_{el} (mb)	Re $f(0)$ (fm)	Im$f(0)$ (fm)
0.050	13.6	13.6	0.0	0.00	-0.504	0.028
0.100	13.5	13.5	0.0	0.00	-0.501	0.055
0.150	13.3	13.3	0.0	0.00	-0.497	0.081
0.200	13.1	13.1	0.0	0.00	-0.491	0.106
0.250	12.8	12.8	0.0	0.00	-0.484	0.129
0.300	12.4	12.4	0.0	0.00	-0.476	0.151

K^+ n

P (GeV/c)	σ_{tot} (mb)	σ_{el} (mb)	σ_{an} (mb)	σ_{an}/σ_{el} (mb)	Re $f(0)$ (fm)	Im$f(0)$ (fm)
0.050	6.8	3.0	3.8	1.27	-0.24	0.014
0.100	6.8	3.0	3.8	1.27	-0.24	0.027
0.150	6.7	2.9	3.7	1.27	-0.23	0.041
0.200	6.6	2.9	3.7	1.27	-0.23	0.053
0.250	6.4	2.8	3.6	1.27	-0.23	0.065
0.300	6.2	2.7	3.5	1.27	-0.22	0.076

K^+ He

P (GeV/c)	σ_{tot} (mb)	σ_{el} (mb)	σ_{an} (mb)	σ_{an}/σ_{el} (mb)	Re $f(0)$ (fm)	Im$f(0)$ (fm)
0.100	160.4	82.4	78.0	0.9	-1.16	0.65
0.200	69.4	42.4	27.0	0.6	-1.27	0.56
0.300	49.4	18.1	31.3	1.7	-1.26	0.60
0.400	46.9	8.3	38.6	4.6	-1.10	0.76
0.500	48.0	5.6	42.4	7.6	-1.00	0.97
0.600	50.1	4.6	45.4	9.8	-0.94	1.21
0.700	50.2	4.1	46.1	11.3	-0.92	1.42
0.800	55.6	4.2	51.4	12.2	-0.82	1.80
0.900	59.8	4.5	55.4	12.4	-0.73	2.18
1.000	64.0	4.9	59.2	12.1	-0.68	2.59

K^+ Be

P (GeV/c)	σ_{tot} (mb)	σ_{el} (mb)	σ_{an} (mb)	σ_{an}/σ_{el} (mb)	Re $f(0)$ (fm)	Im$f(0)$ (fm)
0.100	466.2	302.2	164.0	0.5	-1.88	1.88
0.200	201.4	157.6	43.9	0.3	-2.59	1.63
0.300	132.4	64.2	68.2	1.1	-2.69	1.60
0.400	114.8	31.7	83.1	2.6	-2.41	1.85
0.500	110.8	21.3	89.5	4.2	-2.22	2.24
0.600	112.1	17.2	94.9	5.5	-2.10	2.72
0.700	109.8	14.8	95.0	6.4	-2.05	3.10
0.800	119.5	14.7	104.8	7.2	-1.81	3.86
0.900	127.8	15.2	112.6	7.4	-1.59	4.65
1.000	136.0	16.5	119.5	7.3	-1.50	5.49

K^+ C

P (GeV/c)	σ_{tot} (mb)	σ_{el} (mb)	σ_{an} (mb)	σ_{an}/σ_{el} (mb)	Re $f(0)$ (fm)	Im$f(0)$ (fm)
0.100	607.0	418.6	188.3	0.4	-2.06	2.45
0.200	271.1	218.6	52.5	0.2	-3.14	2.19
0.300	175.9	89.3	86.5	1.0	-3.33	2.13
0.400	148.5	43.6	104.9	2.4	-2.93	2.40
0.500	144.1	29.6	114.5	3.9	-2.67	2.91
0.600	146.5	24.4	122.0	5.0	-2.50	3.55
0.700	145.4	21.6	123.7	5.7	-2.45	4.11
0.800	158.1	22.0	136.1	6.2	-2.15	5.11
0.900	168.3	23.0	145.4	6.3	-1.88	6.12
1.000	178.8	24.9	153.9	6.2	-1.75	7.22

K^+ Al

P (GeV/c)	σ_{tot} (mb)	σ_{el} (mb)	σ_{an} (mb)	σ_{an}/σ_{el} (mb)	Re $f(0)$ (fm)	Im$f(0)$ (fm)
0.100	1010.1	638.6	371.5	0.6	-1.77	4.08
0.200	681.2	570.8	110.4	0.2	-4.76	5.50
0.300	448.6	277.4	171.2	0.6	-5.92	5.44
0.400	349.2	141.8	207.3	1.5	-5.51	5.64
0.500	320.5	96.2	224.2	2.3	-5.10	6.47
0.600	315.5	78.8	236.7	3.0	-4.78	7.65
0.700	308.1	69.3	238.9	3.4	-4.70	8.71
0.800	327.6	68.5	259.1	3.8	-4.07	10.59
0.900	344.3	70.3	274.0	3.9	-3.52	12.52
1.000	362.2	74.8	287.4	3.8	-3.25	14.63

K^+ Fe

P (GeV/c)	σ_{tot} (mb)	σ_{el} (mb)	σ_{an} (mb)	σ_{an}/σ_{el}	Re $f(0)$ (fm)	Im$f(0)$ (fm)
0.100	1520.2	846.7	673.6	0.8	-1.99	6.14
0.200	1392.9	1116.2	276.7	0.2	-6.54	11.25
0.300	971.3	643.3	328.0	0.5	-9.81	11.77
0.400	735.7	342.9	392.8	1.1	-9.76	11.89
0.500	654.5	235.2	419.2	1.8	-9.22	13.22
0.600	630.8	191.9	439.0	2.3	-8.70	15.29
0.700	609.3	168.0	441.3	2.6	-8.59	17.23
0.800	636.8	163.2	473.6	2.9	-7.36	20.58
0.900	662.9	165.6	497.3	3.0	-6.31	24.10
1.000	692.4	174.3	518.1	3.0	-5.77	27.97

K^+ Cu

P (GeV/c)	σ_{tot} (mb)	σ_{el} (mb)	σ_{an} (mb)	σ_{an}/σ_{el}	Re $f(0)$ (fm)	Im$f(0)$ (fm)
0.100	1685.5	919.1	766.4	0.8	-2.25	6.81
0.200	1580.0	1267.8	312.2	0.2	-7.14	12.76
0.300	1111.9	735.1	376.7	0.5	-10.94	13.47
0.400	842.7	397.3	445.4	1.1	-11.00	13.62
0.500	746.7	272.8	473.9	1.7	-10.44	15.08
0.600	717.5	222.1	495.4	2.2	-9.88	17.39
0.700	691.0	193.8	497.2	2.6	-9.77	19.54
0.800	720.4	187.3	533.1	2.8	-8.36	23.28
0.900	749.3	189.6	559.7	3.0	-7.18	27.24
1.000	782.1	199.3	582.8	2.9	-6.55	31.59

K^+ Pb

P (GeV/c)	σ_{tot} (mb)	σ_{el} (mb)	σ_{an} (mb)	σ_{an}/σ_{el}	Re $f(0)$ (fm)	Im$f(0)$ (fm)
0.100	3862.9	2201.6	1661.3	0.8	-3.99	15.60
0.200	3674.3	2720.7	953.7	0.4	-5.58	29.68
0.300	3379.4	2339.1	1040.2	0.4	-16.66	40.95
0.400	2680.0	1498.0	1182.0	0.8	-22.26	43.30
0.500	2307.3	1077.0	1230.2	1.1	-23.53	46.60
0.600	2142.6	876.0	1266.5	1.4	-23.23	51.93
0.700	2019.3	757.6	1261.7	1.7	-23.75	57.10
0.800	2026.6	700.0	1326.5	1.9	-20.05	65.49
0.900	2065.8	689.7	1376.1	2.0	-16.98	75.10
1.000	2124.1	707.2	1416.9	2.0	-15.26	85.80